Online Monitoring Framework for Pressure Transient Detection in Water Distribution Networks

by

Nina Feng

A thesis
presented to the University of Waterloo
in fulfillment of the
thesis requirement for the degree of
Master of Applied Science
in
Civil Engineering

Waterloo, Ontario, Canada, 2019

Author's Declaration

I hereby declare that I am the sole author of this thesis. This is a true copy of the thesis, including any required final revisions, as accepted by my examiners.

I understand that my thesis may be made electronically available to the public.

Abstract

Access to potable drinking water is a necessity and basic human right. Most North Americans obtain treated water through water distribution networks, an essential part of municipal infrastructure that is subject to decay and degradation. Amongst the factors influencing pipe failure are events that trigger abrupt pressure changes, or *transients*, which can cause pipe breakages in the short term, and general fatigue in the long term. The ability to quantify these transients as they occur is important for effective asset management, and for preventing and mitigating the occurrence of failure. Current practices take a largely reactive approach to event detection, and few systems capable of real-time transient detection have ever been implemented.

This research addresses the need for an online monitoring framework aimed towards understanding pressure transient effects and behaviour. The proposed system uses an Internet of Things approach, combining pressure sensors with Raspberry Pi computers, as well as open-source tools that transmit and display the data. The data analysis combines computationally inexpensive methods in order to achieve an accurate decision-making tool for both transient detection and abnormal transient risk identification. The techniques used include different filtering and detrending methods, feature extraction for dimensionality reduction, three-sigma statistical process control, and classification using voting methods. The process also includes a second process, based on statistical process control and trained using transient data identified in the original process, in order to assign a risk for a transient to cause damage, as well as identify transients that are particularly severe.

Data was collected from a unique laboratory water distribution network as well as a field installation in Guelph, Ontario. The results showed that the framework achieves real-time transient identification with reasonable detection and error rates. Further analysis illustrated the effect of factors such as transient source location, active flow in the pipes, and transient type, on transient propagation and detection. The performance of the framework proves the concept of IoT-based systems for pressure monitoring and event detection in municipal water infrastructure.

Acknowledgements

I'd like to express my appreciation first and foremost to my supervisor, Dr. Sriram Narasimhan. I am immensely grateful for having been given the opportunity to move out of my comfort zone, and for the guidance and encouragement that helped me succeed along the way. Thank you so much for taking a chance on an Enviro who knew nothing about structural dynamics, and still doesn't really.

Without quality data and a reliable platform from which data could be collected, nothing useful could have been accomplished in this thesis, or any other for that matter. I owe much of the success of this research to Dirk, whose reliability, work ethic, and knack for solving any and all problems has saved my life on many occasions. Another shout-out goes to Terry, who somehow always came through with whatever part or tool we needed, and never hesitated to teach us how to do things ourselves.

The project also could not have been completed without collaborating with our many industry partners. Thank you to Jim and John with Optys, whom I'll always remember, for gracing us with their patience, knowledge, and personalities. Much of the development of the many different technologies needed for research success can be attributed to Rick and Don with HNSI, Ilia AKA Mr. Robot, as well as Eramosa and Terepac. Much of my appreciation also goes to the City of Guelph, Precision Hydrant Services, and C3 Water for their cooperation with field tests.

My graduate experience wouldn't have been the same without my supportive research group, especially Stan and Roya for their research help, and Dylan for always being motivational.

On a personal note, I'd like to thank my family for always being there: my formidable parents, my wonderful siblings, and my ever-supportive grandparents. I also need my friends, the ones who spark joy in my life, to know that they're very much appreciated for having dealt with me, listened to me, and helped me pass the time as pleasantly as possible.

Dedication

To anyone who ever took a risk, and then struggled.

Table of Contents

List of Tables

List of Figures

Abbreviations

CUSUM cumulative sum

DMA district-metered area

IoT Internet of Things

RMS root-mean-square

SPC statistical process control

WDN water distribution network

Chapter 1

Introduction

1.1 Motivation

Water is one of the most important natural resources for the support of life on Earth. However, the availability of the supply is limited. Canada possesses 20% of the world's fresh water supply but even then, only 7% of that is renewable (Canada, 2017). The responsible use of water is therefore imperative for sustainable human development, and care should be taken to minimize of the loss and waste of an already depleting resource. The vast majority of citizens residing in North America obtain their water through municipal water distribution network (WDN), complex systems of mostly underground pipes that deliver potable water from a treatment plant to the point of consumption residential homes. The maintenance of a healthy pipe network is therefore an essential factor in providing the public with a reasonable quality of life.

Water pipes may suffer damage from a number of different phenomena during their lifetime in a distribution network. The damage eventually leads to pipe failure and can occur over a prolonged period of time, or as a result of catastrophic events. Failure mechanisms resulting mostly from continuous stress include corrosion and pipe fatigue, while others can develop much more suddenly and include circumferential and longitudinal cracking (Folkman, 2012). A study by Folkman in 2018 showed that break rates have been increasing in North America, and have now reached 14 breaks/100 miles/year. Leaks and breakages pose dangers both physical and health-related, disrupt water delivery, result in significant water loss, and are expensive and inconvenient to rectify.

One of the primary contributors to damage-causing stress on water pipes is the occur-

rence of abrupt pressure changes, known as pressure transients. Transients are constantly occurring in WDNs at different levels of severity, and their effect on pipes can be further exacerbated by pipe age, pipe material, and temperature fluctuations. Quantifying the frequency in which they occur, as well as identifying when the magnitude of the pressure change carries a high risk of damage, is important for both preventing and responding to failures exacerbated by pressure.

A monitoring system capable of continuously analyzing pressure data would therefore be very beneficial for WDN maintenance. Very few solutions along these lines have been developed thus far, and current practices consist of mostly routine inspection methods and do not allow for the immediate detection of an event. While municipalities do have proactive asset management plans in place for WDNs, many factors that could be considered when developing pipe replacement schedules have not historically been accounted for, due to lack of knowledge about their effects on pipe longevity.

Traditional methods are further hampered by the impracticality of regularly inspecting all the pipes in a network, allowing failures that are not obviously detectable to develop for longer periods of time. The location of the majority of the water pipes is underground, which poses an extra challenge and reduces the efficiency of many inspection methods. Some parts of a WDN are either remote or otherwise difficult to access, and any issues causing events may remain undetected. There is a need for online, remote, monitoring systems that can communicate status updates and alerts over relatively long distances. Recent research in the direction real-time communication adopts an Internet of Things (IoT) approach, an area that combines data analytic techniques such as machine learning, with sensor-based data collection in an integrated framework.

The development of a real-time monitoring solution with remote communication capabilities would help shift the maintenance philosophy more towards preventative measures and away from reactive failure mitigation. The information obtained would be useful in improving the design and maintenance of WDN, by providing additional insight for decisions such as determining the placement of pressure surge control devices, or planning the replacement of infrastructure. Such a solution would ultimately help to reduce the rate of failure, save time and resources, and mitigate abnormal events in a timely, efficient manner.

1.2 Objective Statement

The overall objective of the research is to develop a useful and practical method for real-time pressure transient detection in water distribution networks that can be used to quantify and provide alerts for abnormal and dangerous transient activity.

1.3 Research Scope

The research described in this thesis aims to develop an event detection system for municipal WDNs based on the IoT concept. The system would perform analysis on pressure data taken from different nodes in order to identify transients. The solution can be applied firstly for background monitoring, in which the frequency of transient occurrence can be estimated in order to study the long-term effects of network water usage on pipe integrity. Secondly, the same system could also function as an alert system in the case of abnormal transient activity, specifically those that could immediately result in pipe failure.

The bulk of the analysis during the research and development stage will be performed on data obtained in a laboratory setting, on a unique test-bed that imitates field conditions in many different ways. A sensitivity analysis will be performed in order to draw conclusions about the effect of different variables on transient detection, which could help in determining future sensor placement and calibration. Once the concept has been proven and modified in the laboratory, the system will also be tested in a lesser capacity in a real municipal WDN, but long-term deployment will not be included in the thesis.

One of the main objectives for the system is to achieve ease and practicality of implementation. The system utilizes mostly open-source technology, both in the computing hardware and the IoT tools. The computing is handled by a small single-board Raspberry Pi computer, which runs through the data analysis at a node-level, before using other open-source tools for the transmission and visualization of the data.

Much of the research focuses on developing an accurate and efficient data processing algorithm, which also demands relatively little in terms of processing power and time. The proposed algorithm therefore combines the use of common and easily adaptable data analysis techniques such as filtering, statistical process control, feature extraction, and voting classification.

Chapter 2

Background and Literature Review

The existing literature is reviewed to understand the problem and the existing solutions. Topics explored and presented in this chapter include a background on the theory and propagation of pressure transients, the techniques for transient identification that have previously been developed, and the state of the art for condition monitoring in WDNs.

2.1 Pressure transients in WDNs

Pressure transients in WDNs can have different causes, occur with varying severity, and are influenced by an assortment of parameters within the pipe network. The behaviour of pressure transients in WDNs will be examined in this section, along with the relevant mathematical equations that have been developed to model such transients.

2.1.1 Transient behaviour and influencing factors

Operating a water transport system involves many factors which have been studied throughout the history of modern distribution systems. In 1984, Kroon et al. posited that a water distribution system can never have a true 'steady-state' or ambient condition. Any activity that alters the the liquid flow rate will result in a force, or pressure transient, that changes the velocity of the flow. Ord (2006) shows that the relative incompressibility of the fluid causes a shock wave of force to travel along the pipe length(s)—, resulting in a pressure transient—which is illustrated in Figure 2.1. In most cases, the kinetic energy of the fluid is converted into strain energy in the pipe walls during a transient event (Boulos et al.,

2005). While most pressure fluctuations are harmless, large and rapid pressure surges, known as water hammers, can cause damage to the pipe network.

The causes of pressure transients in WDNs can include normal events such as general demand and maintenance activities, as well as unforeseen events such as pipe breakages and equipment failure. For the former, water hammers can be caused by operational events including sudden valve closures, pump stoppages, and changes in pressure head at tanks and reservoirs (Boulos et al., 2005). Though infrequent, periods of planned maintenance, such as hydrant flushing or pipe filling and draining, also rapidly change the demand and require transient consideration. Abnormal disturbances that are unplanned, including main breaks and line freezes, can have more serious consequences and the WDN must be engineered to accommodate for such occurrences (Boulos et al., 2005).

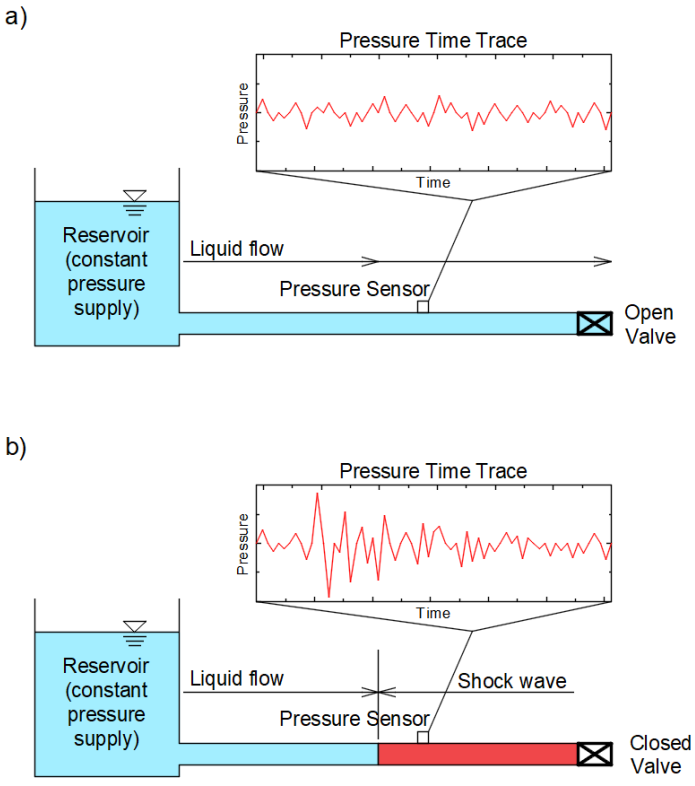

Figure 2.1: Pressure transient development example in a simple pipe system with a valve: a) Valve open, steady flow; b) Valve closed.

Figure 2.1 illustrates the effect of the pressure transient on a pressure time trace as it passes a measuring point. A previously gently fluctuating pressure will experience a sudden drop or spike, followed by an oscillatory behaviour as the system returns to its

steady state (Starczewska et al., 2014). The fundamental equation of water hammer, also known as the *Joukowsky Equation*, relates changes in pressure (ΔP) to changes in velocity (Δv), and was first introduced by Joukowsky in 1898. This relationship can be written as follows:

$$\Delta P = \rho a \Delta v \tag{1}$$

where ρ is the fluid mass density and a is the acoustic (water hammer) wave speed. Korteweg (1878) defines a for the fluid contained in cylindrical pipes of circular cross-section:

$$a = \sqrt{K^*/\rho} \quad \text{and} \quad K^* = K/[1 + (DK)/(eE)] \tag{2}$$

where D is the diameter of the pipe, e is the wall thickness, E is the modulus of elasticity for the wall, and K is the bulk modulus of the contained fluid, which for the purposes of this thesis is drinking water.

Since events in a WDN will inevitably result in positive or negative accelerations in the fluid flow, Equation 1 quantifies the total resultant change in pressure during a transient-causing event. Equation 2 allows for the pipe material and fluid properties to be considered, thus facilitating the application of Joukowsky's equation directly to a WDN. Transient events are very short-lived in water distribution networks, with acoustic wave speeds ranging between 200 to 1250 metres per second, depending on the pipe material (Pothof and Karney, 2013). The events can create massive pressure fluctuations which, given the relationship shown in Equation 1 is directly proportional in magnitude to the high acoustic wave speeds.

While the governing equations can predict the theoretical overall change in pressure, there are a number of other factors that must be considered in a live WDN. Features such as bends, junctions, and other obstacles in complex pipe networks will cause reflections of some parts of the wave (Thorley, 1969), and conditions within a pipe system will affect the attenuation, shape, and timing of the wave. Bergant et al. (2008) studied the effects of dominant parameters influencing wave propagation including unsteady friction, cavitation (i.e. column separation and trapped air pockets), different fluid-structure interaction (FSI) effects, the visco-elastic behaviour of the pipe-wall material, and leakages and blockages. It was found that the presence of most of the parameters caused increased damping, with the exception of certain FSIs and the collapse of large vapour cavities.

2.2 Transient detection techniques

There are various methods that have been studied for the detection or identification of pressure transients in water pipe networks. The transient detection techniques to be discussed focus on data-driven statistical and artificial intelligence (AI) techniques that use pressure data, although other methods are also presented for overall context. It must be noted that there is a lack of detection methods that are transient-specific, and that many of the methods discussed were developed in the context of leak detection. Real time and non-real time methods will be compared for their efficiency and ease of implementation, as one of the main objectives of the research is to employ the transient detection algorithms in real-time. A summary of the research to be reviewed is shown in Figure 2.2.

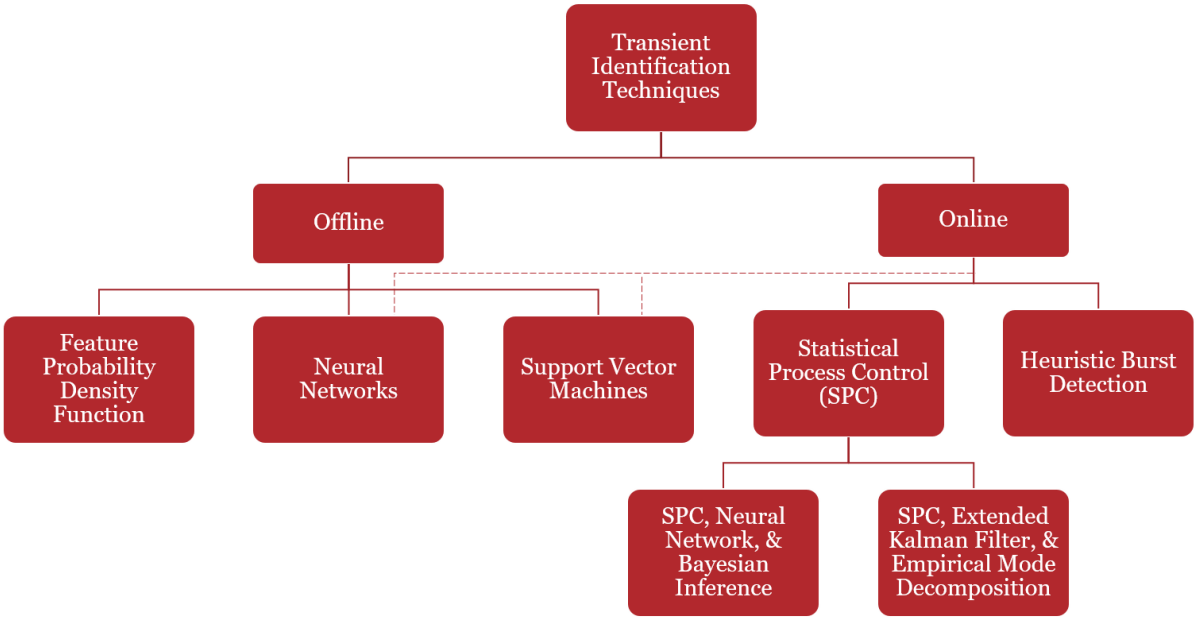

Figure 2.2: Overview of relevant transient detection techniques in literature.

2.2.1 Offline techniques

Offline (non-real time) techniques encompass the basis of transient detection methods in the literature to date, as the development of technology that facilitates real-time processing is relatively recent. Generally, either a large quantity of example data, or accurate physical information from a system, is required for algorithm development. The data is then used to build analytical or data-driven models to which new measurements can be compared.

One of the techniques, used by Gamboa-Medina et al. in 2014, involves using a sizeable amount of sample pressure data in order to calculate statistical features that are then used to build probability density functions to model a system before and after a leak has been introduced, which results in a change in pressure. The following four features were calculated from data sets corresponding to leak and no-leak conditions, in a laboratory test-bed: energy, entropy, zero crossings count, and distribution of energy in the components of wavelet decomposition. The technique aims to detect pressure transients resulting from the onset of leaks, and it was determined that feature comparison techniques could be an effective tool for transient identification. Most importantly, combining information obtained from different features increased the accuracy of classification.

Machine learning algorithms can also make use of existing system data, where previously obtained data is used to train a classifier to recognize the presence of a pressure transient. Mounce and Machell (2006) showed that artificial neural networks (ANNs) could be applied in order to identify and pressure transients from bursts, using pressure and flow time series data. Two different architectures were used - a static neural network and a time delay neural network - in which the latter was found to be more accurate due to its context memory. The data, obtained in a UK WDN, was filtered and normalized before being input into the ANN, and it was found that the method's effectiveness depended on the data quality and sufficient exemplars for training. Further research (Mounce et al., 2014) applied a pattern matching technique along with a binary neural network to recognize waveforms caused by transients and other disturbances in several parameter time signals. It was found that although the binary neural network was highly proficient, the pattern matching was constrained by the requirement of a manually-populated waveform library that could not identify previously unencountered events.

Support vector machines (SVMs) have also been used in transient detection and have produced promising results for the prediction of leaks and their locations. Mashford et al. (2009) found that SVMs produced accurate classifications for leak detection trained and tested on data simulated from the EPANET hydraulic modelling system. Field testing was then conducted by Mounce et al. (2011) and it was found that SVMs had the potential to perform faster than the ANN system (Mounce and Machell, 2006) and that it could enable automatic online processing in the future.

A number of offline techniques have been shown to provide accurate results for transient detection. The ability to obtain the appropriate data for training is imperative to how well different methods work. For this reason, few techniques have been commercialized for

actual WDNs, due to the abundance of limitations that make them impractical for real applications.

2.2.2 Online transient detection techniques

Online (real time) techniques allow for the near-instantaneous detection of pressure transients as they occur in a WDN. As a relatively new realm of study, the literature reviewed in this section focuses on techniques that can be implemented continuously on an incoming data stream, which makes them particularly useful for transient detection, as they can occur and travel very quickly.

Several of the techniques explored in the literature employ statistical process control (SPC) methods in their analysis schemes. Originally used for quality management in manufacturing, SPC is comprised of various statistical tools that monitor different process parameters in real-time, in order to control system variability (Doty, 1996). It can be used in combination with many traditionally offline methods in order to conduct real-time classification.

Misiunas et al. (2005) built a real-time break detection and localization algorithm around the use of cumulative sum (CUSUM), an SPC feature which allows for the sequential analysis of a data stream to detect abrupt changes. The method is used on data that was pre-filtered using an adaptive recursive least-squares (RLS) filter, and compares the measured pressure signal to a pre-calculated pressure change corresponding to the minimum break size. It is important to note that after the initial change is detected, more detailed analysis needs to be performed offline on the corresponding window of data. While the first phase of detection employed a one-sided CUSUM test, the detailed analysis uses a two-sided test (i.e. both the positive and negative changes are analyzed). The data is filtered using a Butterworth low-pass filter and the duration of the initially detected transient and any subsequent reflections is used for break localization. The technique showed that SPC methods including CUSUM are effective in WDN pressure transient detection, but that it is prone to false alarms and sensitive to normal changes in system conditions. The need for offline validation, two filtering methods, and adaptive data tuning also decreases its efficiency as a real-time transient identification system.

A more sophisticated process was developed by Romano et al. (2014), which not only uses SPC for short- and long-term analysis of anomalies and variations, but also wavelets for signal de-noising, artificial neural networks (ANNs) for short-term signal forecasting,

and Bayesian inference systems (BISs) for inferring the probability of a pipe burst/other event occurrence and raising corresponding detection alarms. The method also draws upon ANN work done by Mounce and Machell (2006), an offline burst identification system. The result was a technique that minimizes the false alarm rate and maximizes accuracy. The method takes much more processing power than simpler techniques, and the detection time is not instantaneous, as it uses 15-minute intervals for data recording. Typically, events are identified within an hour of occurrence.

A heuristic burst detection method with a much faster processing time was developed by Bakker et al. (2014), and was found to reduce the rate of false alarms when compared to the SPC method. Instead of using pressure data, the water demand (presented as a flow rate) is used, which is calculated by doing a water balance in a district-metered area (DMA). However, the technique is achieved by continuously comparing the measured demand signal in real-time with a forecasted signal derived from 5 years worth of data. The extensive amount of historical information needed for the method to work makes it difficult to implement and also sensitive to future overall increases or decreases in demand.

Jung and Lansey (2014) indicated that SPC methods had limited effectiveness when used in systems that undergo operational changes when engaging or disengaging components such as pumps, valves, and tanks. The pressure signal becomes discontinuous, and false alarms would be a regular occurrence for such systems. An extended Kalman filter (EKF) method was suggested, which is a model-based approach that continuously forecasts and updates data in various nodes across a WDN. The method can successfully account for different system dynamics, however the need for specific information about the network components may add difficulty for the scaling and implementation of the method in larger, more complex WDNs.

The need for online pressure transient identification techniques has been recognized and explored. Several different methods have been attempted, each with their advantages and disadvantages. Simple and easily implemented techniques have a high rate of false alarms, while more sophisticated techniques use a large amount of processing power and often cannot achieve true real-time transient detection. On the other hand, approaches that use less processing power and achieve faster transient identification often require substantial *a priori* information to implement.

There is a need for a solution that can function mostly unsupervised that minimizes speed and processing power, while maximizing accuracy in transient detection.

2.3 Condition monitoring in WDNs

Condition monitoring practices for WDNs are important for the prevention, detection, and mitigation of issues that may affect the health of the networks. Current practices, as well as state-of-the-art methods under development, can be classified into either periodic maintenance and inspection techniques, or real-time data-driven methods. The following is a summary of the technologies that have been adopted by municipalities for water infrastructure analysis, as well as new methods that have been more recently developed to allow for real-time continuous monitoring.

2.3.1 Common current strategies

Rizzo (2010) summarized the approaches and technology used for nondestructive evaluation (NDE) and structural health monitoring (SHM) in WDNs. Methods discussed included visual inspection, the use of pipeline inspection gauges (PIGs), electromagnetic methods, ground-penetrating radar, hammer-sounding, sonar, and magnetic flux leakage. Due to the labour required for their implementation, these methods are used only periodically for regulatory compliance and often on a more reactive basis, and none provide continuous monitoring for the timely detection of events.

Virtually the only widely used systems that have real-time monitoring capabilities are Supervisory Control and Data Acquisition (SCADA) systems, which collect information on flow rate, pressure, and water quality. Despite the functionality, the vast majority of the monitoring stations are located at reservoirs, water tanks, and pumping stations (Dobriceanu et al., 2008), which does not allow for network-level monitoring.

Generally, it can be said that most municipalities do not yet have tools available for remote and continuous data collection relating to conditions in WDNs.

2.3.2 Smart infrastructure and Internet of Things

Data that can be collected in a WDN can be useful for maintaining the long-term health of a system. Real-time condition monitoring in WDNs typically aims to detect events in the network, and also to further identify abnormal behaviour within the events.

Recently, the lack of smart condition monitoring in WDN infrastructure has been recognized and some solutions have been developed, with a select number being implemented in

live WDNs. WaterWiSe (Whittle et al., 2013, 2010; Srirangarajan et al., 2010) is a platform that has been tested in Singapore, building off a smaller-scale endeavor in Boston called PipeNET (Stoianov et al., 2006). Both platforms employ a network of micro-controller-governed, time-synchronized hydraulic and water quality sensors equipped with a means for data transmission, and both were tested extensively in a field environment. An example of an IoT framework (Robles et al., 2015), the WaterWiSE framework uses a node-to-server architecture that collects data at the node level and sends it to the servers for further processing. The servers use wavelet decomposition and time-domain statistical analyses are used on the pressure trace for transient detection and alerting. The processing algorithms were proven to function fairly well, but were computationally expensive. The system requires an extensive back-end processing unit that actually utilizes three servers: a web server, a data archive repository, and a processing server (Whittle et al., 2010).

Other research endeavors for anomaly or leak detection include SPAMMS (Sensor-based Pipeline Autonomous Monitoring and Maintenance System) (Kim et al., 2010) that made use of a combination of fixed and mobile robotic sensor nodes, and SmartPipes, (Sadeghioon et al., 2014), that used sensor clamped around water pipes. Both systems conducted some data pre-processing at the node level, and were tested on their respective laboratory test-beds, which were smaller in scale than a municipal WDN. The SPAMMS framework was fairly complicated while SmartPipes used more rudimentary detection methods, but both would be physically difficult to implement in a real WDN.

The development of strategies that can be commercialized for municipal use has been rather laborious and with limitations, but new technology has gradually begun to replace or support the accepted methods.

2.4 Summary of limitations and knowledge gaps

The limitations common to the research conducted in the existing literature is compiled in this section, and the resultant gaps in knowledge identified.

2.4.1 Transient identification

The effectiveness of the transient detection methods found in the literature can be evaluated using the following criteria:

- **Speed of identification** For our evaluation, the speed refers to the timeliness in which a transient that has developed would be detected. The causes of large transients in a WDN can vary, but in cases where investigations and corrective actions may be needed, the immediate detection of a pressure transient better facilitates corrective action.

- **Accuracy** The ultimate goal for any transient detection technique is to be able to accurately identify transients, especially abnormal ones, and minimize errors in classification. Preference is given to techniques that yield lower rates of false negatives or positives.

- **Efficiency** The efficiency of a technique can be considered to be a function of the processing power needed for its operation. Techniques that require a lot of processing power can be time-consuming and complicated, and are therefore less ideal than more efficient techniques.

- **Ease of implementation** The ease of implementation is concerned with how much information is needed for the technique to work, and how accurate or high quality the information needs to be. Techniques that require a large amount of accurate data for calibration prior to operation are less favourable than those that don't.

Due to their nature, offline techniques are likely to be slower to implement compared to online techniques. Their accuracy, however, can benefit greatly given that their implementation is not constrained by time or power, but often this results in a lower efficiency. While they have the potential for high accuracy, it can be difficult to achieve due to the uncertainties involved in their implementation and proper calibration.

Online techniques are faster for transient detection, simply because they are being continuously implemented. The shortcomings of these techniques are very similar to those of offline data-driven techniques, as they are implemented with the same principle approaches. However, the ability to detect transients virtually in real-time is a very powerful feature that sets them apart for use in practical applications.

2.4.2 Condition monitoring

As noted in the above review sections, there has been significant progress in developing event detection systems that successfully integrate real-time sensing, event detection, and

IoT. Nevertheless, improvements can be made in order to expedite the adoption of such systems. The frameworks identified during the review conduct the majority of their data analysis in a central environment that receives data from remote sensor locations. Not only can this slow down communication and drive up data transmission costs, but this structure also requires more powerful server-type hardware in order to receive, store, and process the data. There is a need for systems with more node-based processing that decrease data transmission overhead and also schedule computing tasks across multiple locations

Chapter 3

Methodology

Pressure data taken from a live WDN is essential for the validation of the proposed transient identification framework. To facilitate real-time event detection, the system architecture for the framework was designed such that sensing and data analysis occurs in real-time at the node, thereby reducing data transmission costs and allowing for early decision-making. The results of the analysis are then transmitted as status updates for users to view using IoT platforms.

To a ensure a sufficient variety of data, experiments were conducted in both laboratory and field settings. The laboratory test-bed is especially important for conducting detailed validation tests and technique development. The construction and arrangement of a laboratory test bed is presented, as well as the layout and nature of the field test locations. The deployment of the device in both environments is detailed, with specifics about the test plans that guided the experimental procedures.

3.1 System architecture

The development and functionality of the different components of overall system will be summarized in this section, as well as how they work together in real-time to achieve transient detection and alerting using pressure data.

3.1.1 General overview

The data processing system consists of three main elements: sensing, data analysis, and communication. Emphasis was placed on using a small, open-source, and easily accessible computer that could both act as the core of the sensor node, and also handle the bulk of the computing power. The system therefore centres around a Raspberry Pi, and the data processing is completely carried out at the device level, allowing for more immediacy in transient identification and alerting. The burden on back-end servers dedicated to data storage and processing is therefore now reduced, as data reduction processes will be been performed prior to transmission and storage. The general layout of the overall system is illustrated in Figure 3.1. The system integrates both commercially available hardware and IoT platforms, as well as custom PCBs and programming.

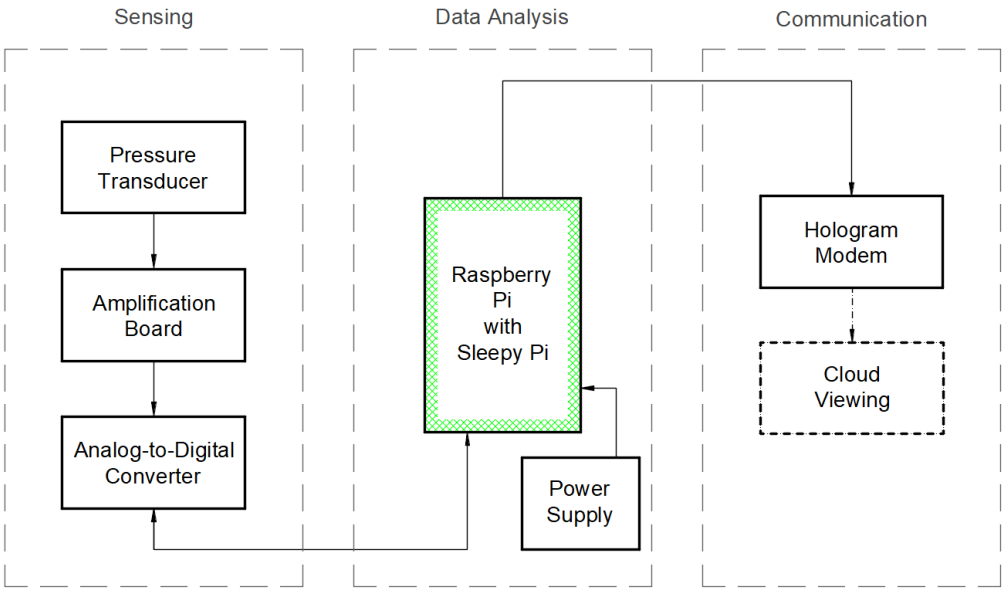

Figure 3.1: Diagram of node hardware architecture.

The Raspberry Pi 3 (RPi) acts as the core controller that governs the other processes. The peripherals attached for sensing use SPI (Serial Peripheral Interface) communication ports on the Raspberry Pi to relay real-time raw pressure signals. The RPi then executes the proposed transient detection algorithms on the incoming data stream and makes decisions with regards to the identification of a transient. The status updates are then transmitted using commercially available IoT solutions where they can be viewed live by an operator. The main physical components of the RPi-controlled device are summarized

in Table 3.1.

It is important that power requirements are minimized in order to facilitate long-term field deployment. The whole system is powered by a rechargeable battery pack that does not need frequent replacement under regular conditions. Furthermore, the RPi can also be placed on a semi-continuous sampling schedule when the need for constant sensing is low. The computer is fitted with a Sleepy Pi shield, an add-on board that can be programmed using the Arduino IDE. The board makes use of a built-in RTC (real-time clock) that controls power to the RPi according to user-programmed times set times. This conserves energy by allowing the system to autonomously enter into sleep/low-power mode when not in use.

Table 3.1: Main device hardware components

Component	Brief Description
Raspberry Pi 3 Model B	Single-board computer.
Sleepy Pi 2	Add-on board for power management.
Honeywell Model S Pressure Transducer	Flush diaphragm pressure sensor.
MCP3302 ADC	13-bit, low power ADC.
Hologram Nova 2G/3G Modem	Open source USB cellular modem.
Boston Power Swing 5300 Battery Pack	6 x 3.65 Volts.

3.1.2 Sensing

The primary component used for data sensing is the Honeywell Model S pressure transducer, a passive sensor whose data sheet can be found in Appendix A. The sensor is constructed using a flush diaphragm, which minimizes buildup and bacterial growth, prolonging the service life as well as being sanitary for drinking water systems. The subminiature size allows for its use in small pressure chambers or thin pipes where space is limited or shared with other hardware.

There are two main sub-processes that occur in the device peripherals during sensing: amplification and analog-to-digital conversion, both of which are needed in order to

transform the raw sensor input into usable data for analysis on the RPi.

During preliminary laboratory trials, it was found that the amplitudes in the pressure time series data were too small for meaningful analysis. With an output sensitivity of 2mV/V at maximum excitation, the electrical signal from the sensor did not show sufficiently large magnitudes of variation, especially during transient events that were smaller in scale. A board was therefore iteratively developed using an operational amplifier for the amplification of the sensor output.

After amplification, the signal needs to be converted from analog to the digital domain. This is accomplished using the MCP3302 ADC, whose data sheet is also in Appendix A. The ADC allows for 12-bit resolution, and is user-programmable with the RPi's existing SPI code framework. Its low consumption of power lends itself well to battery-powered remote data acquisition applications, and is ideal for using the RPi's maximum power output of 5V.

The need to convert the values from voltage to absolute pressure is unnecessary for the transient detection algorithm, as the relative changes to the pressure are more relevant. However for display purposes, a basic 3-point calibration was performed in the laboratory using a pressure gauge as reference, which generated an approximate conversion from the voltage output to the RPi (x), which has a 0-5 V range, to the pressure (P) in pound-force per square inch (psi):

$$P = 83.48x - 176.42 \tag{3}$$

All raw voltage values shown in the thesis are converted to pressure using Equation 3, with no effect on the algorithm performance.

3.1.3 Data analysis

The pressure data from the sensing activities, divided into 0.5 second intervals, is subjected to several analysis tasks performed directly on the Raspberry Pi. The analysis techniques can be grouped into four main processes: data pre-processing, extraction of statistical information (features), anomaly detection through SPC, and final classification. The result is the identification of transient or transient-like phenomena in a data stream. Additionally, a modified version of the SPC anomaly detection can be applied again in order to separate abnormal transient activity from the identified transients. The development and implementation of the data analysis procedures are outlined in this section.

3.1.3.1 Raw data and pre-processing

Preliminary validation tests were performed to test the sensing functionality in conjunction with the data analysis techniques. Results from laboratory and field tests exhibited some unforeseen signal components that hindered the immediate implementation of data analysis algorithms. In both data sets, the presence of a dominant low-frequency pressure wave due to natural pressure fluctuations from WDN operation masked the effects of the induced transient activity. The pattern was most visibly apparent in the laboratory setting, but was also exhibited in the field data. A breakdown of the frequency content in the pressure data taken from both settings showed a very large concentration of energy at frequencies below approximately 4 Hz. Additionally, the field trials produced very noisy signals that masked the frequency components relevant to transient detection. The laboratory data was generally cleaner, but the device was found to be susceptible to background electrical interference in some cases, as demonstrated by the presence of a relatively large 60 Hz peak in the FFT.

Data pre-processing techniques were consequently implemented in order to address the issues and prepare the data for analysis.

Detrending by zero-centering The anomaly detection techniques to be used in the analysis are most concerned with detecting significant deviations from the norm. Normalizing the data is essential to simplify calculations and to produce signals that can be compared under different circumstances. Detrending processes remove any gradual tendencies caused by either electronic drift or changes in background conditions, and in this case, the process of zero-centering simplifies data comparison by shifting all data sets about the mean of zero.

Detrending by filtering The FFT analysis performed on the laboratory data confirms that there are no spectral components of interest at frequencies above 60 Hz. Hence, major unwanted frequency components, specifically resulting from the low-frequency variations occuring below 4 Hz and electrical interference issues occurring above 60 Hz, are then removed using a Butterworth bandpass filter with cutoff frequencies at 4 Hz and 60 Hz. Sela et al. (2018) found that a sampling frequency of as low as 64 Hz could be used while maintaining adequate resolution for statistical modelling. The techniques used for the detection of anomalies in the pressure signal require that the desired frequencies remain relatively unaffected during pre-processing. When compared with other commonly used

filter types, the Butterworth filter maximally flattens the frequency response within the passband and rolls off to zero outside the stopbands, which maximizes the preservation of the signal.

Due to the application of the upper stopband in the filter, the sampling frequency used for sensing on the RPi was re-evaluated. Initially, a sampling frequency of 2048 Hz was used in order to account for both high and low frequency components in the transient analysis. However, since the validation trials have demonstrated fairly inconsequential spectral components in the high-frequency ranges, the maximum frequency, or Nyquist frequency, that is required from the signal is 64 Hz, which corresponds to a sampling rate of 128 Hz on the RPi. The power requirements for the RPi are also reduced as a result of this lower sampling rate.

3.1.3.2 Feature extraction and selection

A set of time series data is essentially composed of a set of values organized in time order. Analysis of just the values in their original state can be inefficient and cumbersome, therefore specific statistical information, or *features*, are extracted instead. Feature extraction acts as a dimensionality reduction technique, where the vector of features acts as a summary description of the time series. A set of features should be non-redundant but representative of the data, and can be used instead of the original data set during analysis.

The initial feature set consisted of various statistical properties commonly used for anomaly detection in signals, as well as from existing leak detection literature such as those presented by Gamboa-Medina et al. (2014). A subset of eleven features that show sensitivity to transient events were chosen for use in the transient detection algorithm, and are shown in Table 3.2. The list includes some common useful features as well as measures of asymmetry, unpredictability, and energy. A *feature vector* containing all eleven values is extracted for every half-second interval. Based on the validation time series, the selected length of the time intervals (0.5 seconds) is sufficient for the capture of multiple cycles of a transient wave, but short enough that the event is not diluted nor that most non-abrupt fluctuations are misidentified.

The use and calculations for the listed features can be found in Appendix B. Some of the features that were considered but ultimately removed from the final analyses include the pulse factor, margin factor, and crest factor. The standard deviation could also be omitted because the detrending and zero-centering of the data renders it fundamentally

Table 3.2: Transient detection feature set

Features		
Maximum	Zero-Crossings Count	Entropy
Minimum	Skewness	Cumulative Sum (Upper Threshold)
Mean	Kurtosis	Cumulative Sum (Lower Threshold)
Root-Mean-Square	Energy	

redundant to the RMS feature. The values in each interval were also checked for cross-correlation. However, it was found during preliminary validation that, while the filtering process removes the dominant signal components that obstruct the analysis, there are still trends in the mean that remain. This reduces the usefulness of checking for cross-correlation, because there still remains correlated values even within the ambient noise.

3.1.3.3 Anomaly detection and classification

The identification of a transient event once a feature vector is calculated is carried out with an SPC-based technique, which is commonly used and easily implemented. SPC focuses on identifying variations in a system from pre-determined normal operating conditions, by means of statistical comparison.

A sufficiently large set of baseline data is first obtained from the WDNs under conditions free of abnormal transients. A large data set ensures the accurate representation of the system, and accounts for typical pressure fluctuations resulting from distribution and demand, thereby reducing the risk of overestimating the frequency of transient activity. A vector containing the mean value from every feature across the training data becomes the feature vector used for training the transient detection algorithms to recognize regular operating conditions.

From the training feature vector, an upper and lower threshold for acceptable values is calculated using *three-sigma (3σ) limits*, meaning that the limits are three standard deviations from the mean (Doty, 1996). The resultant band of acceptable values follows the conventional heuristic reasoning that nearly all, or more specifically 99.7%, of the values in regular conditions will fall within the limits, as illustrated in Figure 3.2. The

rule is derived from properties of normally distributed data, but is still effective for use for non-normal distributions. It can be assumed that most of the features will tend towards a normal distribution because, regardless of the distribution of the original data, the Central Limit Theorem states that statistical properties calculated from samples of a data set should be normal. New data can now be compared against the thresholds to determine whether or not an abnormal pressure change, or transient, has occurred.

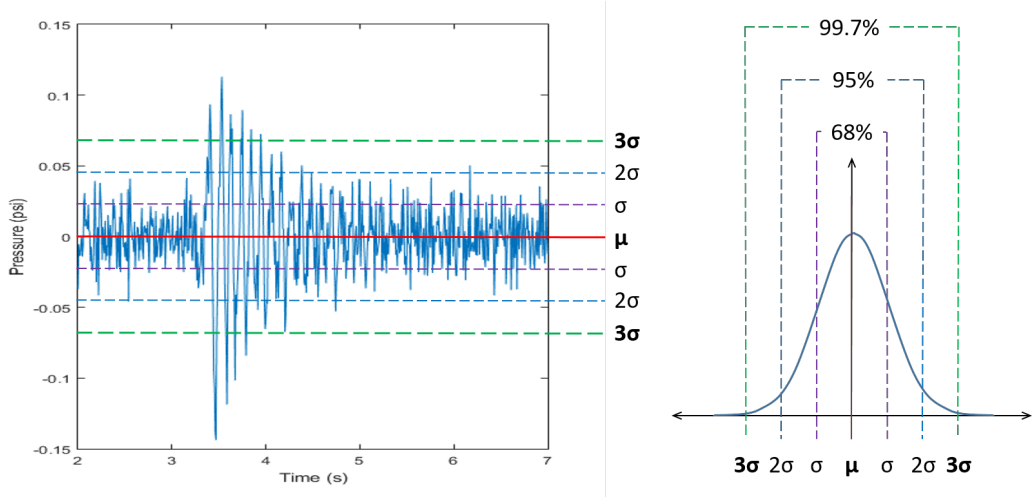

Figure 3.2: Three-sigma thresholds illustrated on an example pressure time trace and on a normal distribution.

The final classification of a pressure transient, or lack thereof, uses the ensemble of features in a majority voting method, The number of features within each time interval that exceed their respective three-sigma thresholds are counted, and the total number is used to determine whether or not a transient had occurred within the interval. Combining the decisions obtained by each feature comparison reduces the sensitivity of the overall identification technique to misidentifications in individual features. Time intervals in which a transient has occurred are expected to have more features that exceed the calculated limits. Numerous exceedances in multiple successive time intervals is also indicative of a genuine transient event.

3.1.3.4 Anomaly detection and classification for abnormal transient detection

A similar SPC process can be used specifically for identifying and assigning severity to abnormal transients, especially those that can cause immediate harm to a WDN. In essence, a two-tier SPC process is used, wherein the first tier separates the transient events from

ambient data, and the second tier separates abnormal transients from regular transient activity resulting from general WDN use.

While ambient flow data is used to train the algorithm in the initial process, the second tier uses the features themselves, taken from the time intervals identified in the first tier as having experienced a pressure transient. The time intervals used in the analysis are not separated out by feature vote threshold yet, and include all intervals in which any number of features were triggered, with the exception of those that were determined to be false positives. In doing so, it is assumed that the most pertinent regular transient types are encompassed, including those induced specifically for the test, and subsequently that statistically significant feature exceedances correspond to abnormal transients.

Not every feature will be deemed suitable for training purposes in SPC, with the primary qualifier being the normality of their respective data sets. This is because part of the purpose of the detection of abnormal transients is to alert WDN operators the occurrence of pressure fluctuations that may require timely attention. Conservativeness in transient identification is important in order to ensure that virtually no false alarms are triggered by the system, in order to minimize wastage in time and resources. Therefore, it is more efficient to use only the features that can classify transients with a high degree of accuracy, and when using sigma methods in SPC it is most optimal to use normally or near-normally distributed data.

While the Central Limit Theorem had established that features calculated from the data would be normally distributed, this is no longer the case with the subset of the features associated with the detected transients. This subset is effectively a truncated portion of the parent normal distribution, and hence it is no longer inherently normally distributed. Tests for normality on each of the transient feature subsets can be conducted by applying probability paper plots, and the features that exhibit normality are selected for use in identifying the abnormal transients. In some cases, a distribution may be transformed from non-normal to normal using power transforms, most notably the Box-Cox one-parameter transform (Box and Cox, 2018).

The resulting probability distributions of the features can be used to evaluate data from the time intervals that have been identified as having transients, in order to obtain a percentile value in which the data falls, for each feature. The average of these percentiles can be used to assign a rank, or level of severity, to the detected transients. The severity should be calibrated for different cases, but a theoretical example is summarized in Table 3.3.

Table 3.3: SPC-based classification of transient behaviour and severity

Statistical bounds	Percentile (%)	Behaviour Type	Transient Severity
μ - 1σ	0 - 68	Regular	Low
1σ - 2σ	68 - 95	Regular	Moderate
2σ - 3σ	95 - 99.7	Regular	Large
$3\sigma+$	99.7 - 100	Abnormal	Extreme

3.1.4 Communication and Internet of Things

The final objective of the transient detection system is to facilitate the early diagnosis of significant and abrupt changes in the WDN pressure through prompt operator alerts. The communication and IoT cyber-architecture is summarized in Figure 3.3.

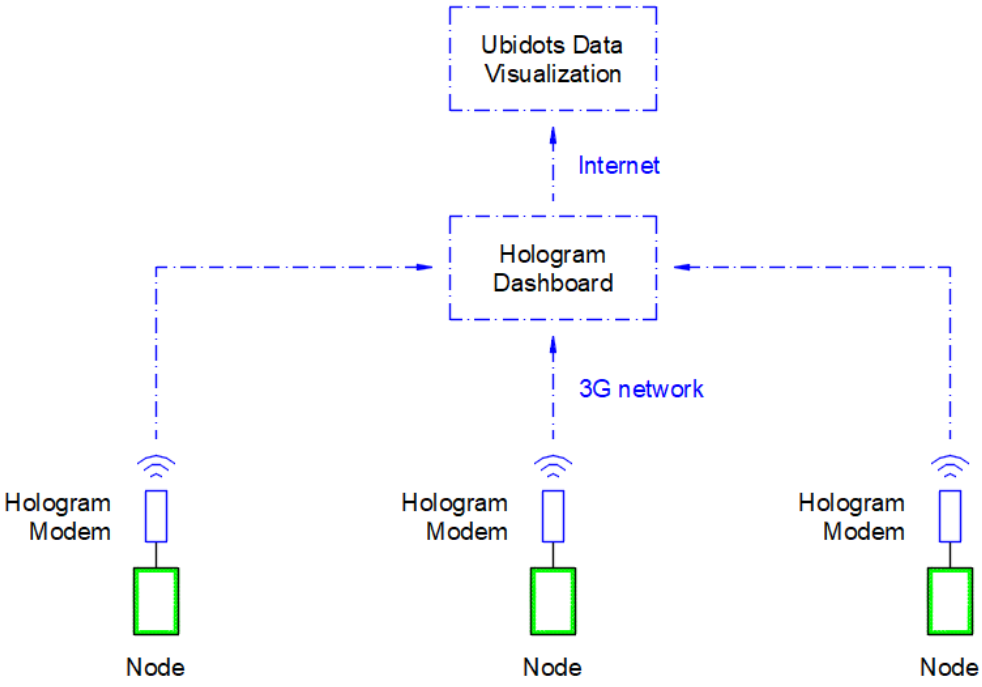

Figure 3.3: Diagram of Internet of Things architecture.

In the event of a positive transient identification, the RPi program transmits a noti-

fication to a cloud hosted by Hologram, an IoT development company. Transmission is handled by the Hologram Nova, an open source cellular modem originally designed for the Raspberry Pi operating system. The device operates off of the u-blox SARA-U201 modem family, which enables the connection to the RPi via USB port and has a maximum data rate of 480 Mb/s. Using a 2G/3G connection from an activated SIM card, SMS data packets can be sent and viewed on the Hologram Dashboard. The messages can be tagged according to subject, and organized by device.

The main purpose of the Hologram Dashboard is the management of the device statuses and transmissions. However, the visual display and organization of the data is not yet supported. This is done instead on the Ubidots platform, which specializes in data analytics and visualization for IoT frameworks. In order to reduce data transmission costs, regular system updates are not being sent. The full data sets are stored locally on each Raspberry Pi, though feature vectors can be sent in the event of a transient identification. The platform is capable of transforming Hologram data packets that could contain pressure values during transient events or otherwise, and display them graphically for the visualization of the SPC control chart, including the thresholds. An example of the user interface (UI) both Hologram and Ubidots is shown in Figure 3.4. Both platforms allow for extensive user customization through their developer tools and provide APIs that easily allow for their adaptation to the transient detection system.

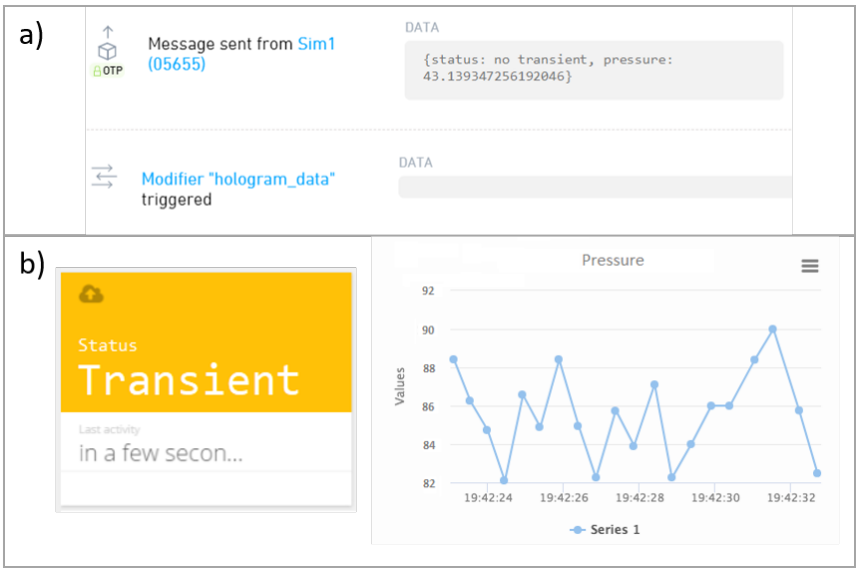

Figure 3.4: Example of Internet of Things user interface: a) Hologram data packets, b) Ubidots data visualizatio.n

3.2 Experimental procedures

In order to develop an effective test matrix for the data analysis algorithm, different conditions and transient scenarios must be considered, both in the laboratory and in the field. Experimental validation and sensitivity analyses were conducted on a novel laboratory pipe network test bed, with operating conditions representative of a municipal WDN. Laboratory test data was used to develop and calibrate all data analysis techniques, including pre-processing, feature extraction and selection, and classification methods. Additional validation for the proposed system was performed in a series of field tests in a municipal DMA.

3.2.1 Laboratory experiments

3.2.1.1 Laboratory set-up

A lab-scale WDN system was built in the Hydraulics laboratory and measures were taken to maintain a reasonable representation of field conditions (i.e. municipal WDN) conditions. The water inlet valve is directly connected to a city water supply in order to provide a steady and reliable pressure that averages at 55 psi, which is within the government guideline pressures of 40 to 100 psi for municipal WDNs Ontario MOECC (2008). A pipe diameter of 6 inches was selected for the pipelines, which also meets the minimum water main diameter guidelines and is fairly common in residential DMAs. The use of Grey Scale 80 PVC as the pipe material allows for more flexibility in the configuration since the lighter and widely available material lends itself well to alterations and maintenance.

Two different pipe configurations were used. Figure 3.5 shows the original configuration, which was used primarily for algorithm validation and modification. The expanded configuration shown in Figure 3.6 is used for a more detailed sensitivity analysis, and contains system features such as bends and junctions, as well as a recirculation loop.

For the laboratory setups, the pressure transducer is housed in a pressure chamber that is attached to the pipe using a one-inch valve connection. The pressure chamber is used because it allows for easier accessibility to the transducer for maintenance and repair, as it would not require the de-pressurization or partial draining of the system, which is especially inefficient when considering municipal WDNs. The one-inch valve can be closed during maintenance, eliminating disruption to the WDN as a whole. The pressure chamber

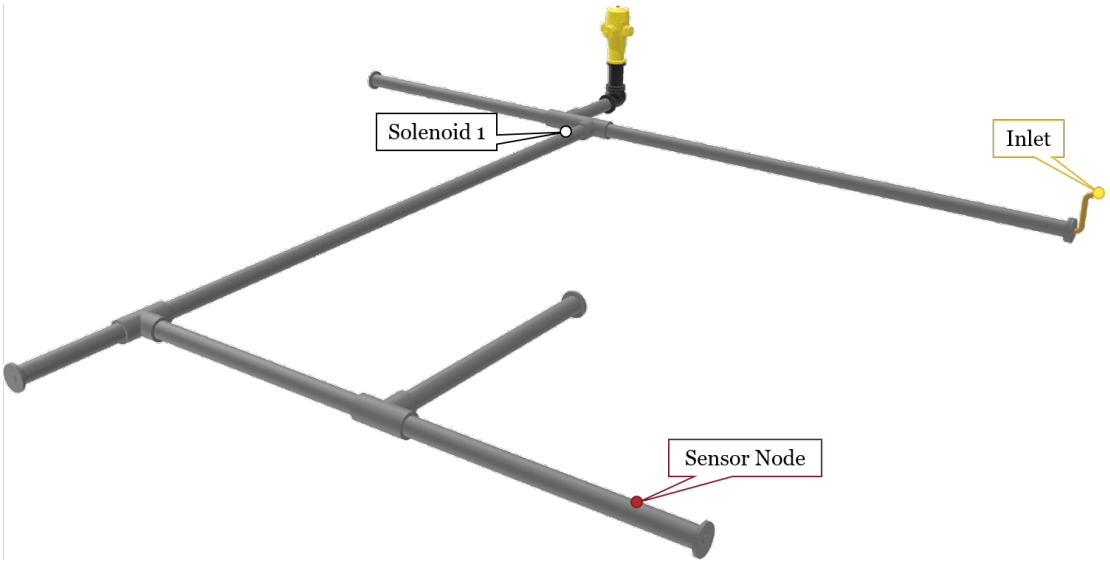

Figure 3.5: Perspective view of initial laboratory configuration.

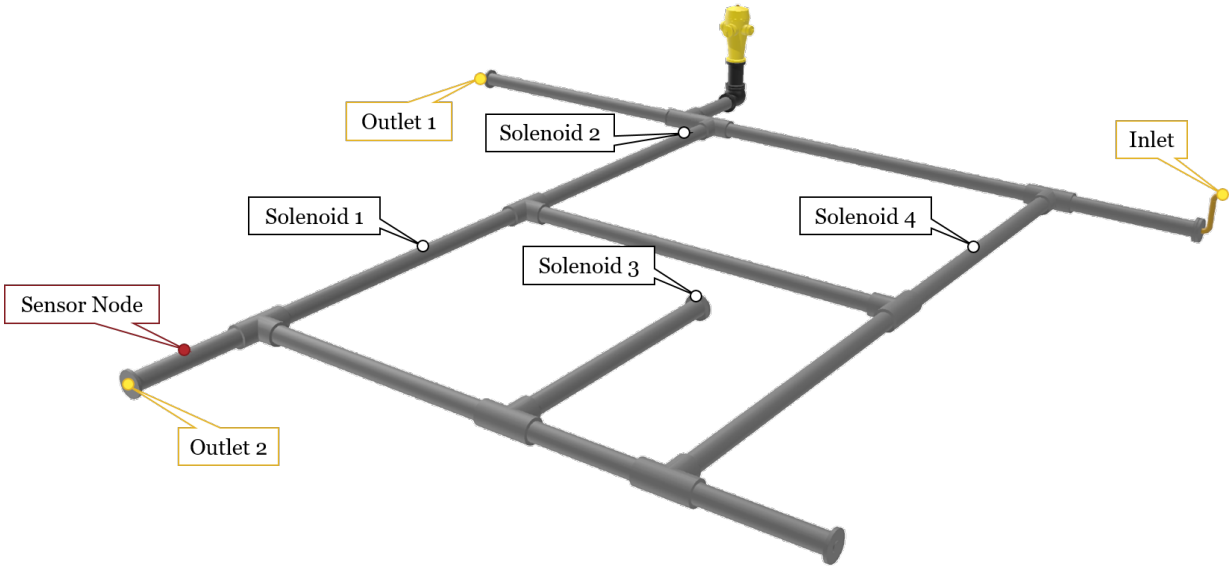

Figure 3.6: Perspective view of expanded laboratory configuration.

hardware also includes housing for the RPi sensor device that is connected to the pressure transducer. A diagram of the chamber is shown in Figure 3.7.

The WDN includes several quarter-inch (1/4") valves at various locations that can be used to simulate small leaks, as well as larger 1.5" outlet valves at pipe endings that can simulate large leaks, water usage, or flow conditions. The transients themselves can be induced using any of the valves, but in order to ensure an abrupt pressure change

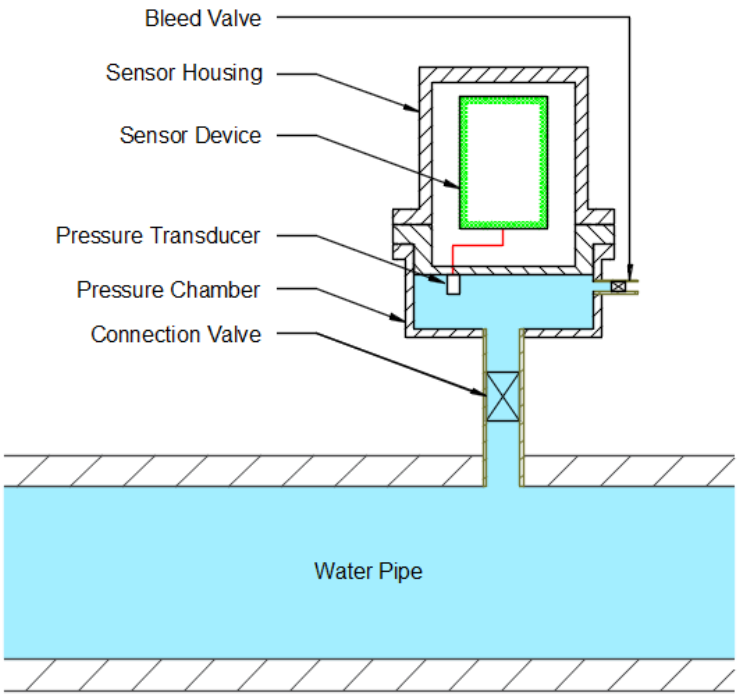

Figure 3.7: Cross-sectional view of sensor pressure chamber.

representative of event-like behaviour, a solenoid valve is used. The solenoid valve is programmable and can be opened or closed near-instantaneously, and the resultant pressure response can be recorded at the pressure chamber.

3.2.1.2 Laboratory test plan

The laboratory test plan attempts to simulate different transient scenarios, producing different signals for the transient detection algorithms to analyze. The sensitivity of the algorithm performance to changing conditions will be analyzed by varying different system parameters, broken into three categories:

1. Transient induction method, where different types of transients can be induced with respect to the solenoid valve position, as shown in Figure 3.8:
    - Closed to Open, where the solenoid valve is opened during the test;
    - Open to Closed, where the solenoid valve is closed during the test from a previously open position; and

- Pulse, where a quick closed-open-closed pattern is induced. A pulse, 50 ms in duration, was selected during testing.

2. Flow conditions, which is split into two modes:
   - No Flow, where the two 1.5" outlet valves are closed; and
   - Flow, where the outlet valves are open.
3. Transient source location, which varies the proximity and number of connections between the transient source and the sensor by changing the solenoid valve's placement in the system. This is translated into the laboratory configuration as follows:
   - Case 1, where the source and sensor are in line but separated by two junctions;
   - Case 2: source and sensor are in line but separated by one junction;
   - Case 3 where the source and sensor are separated by two junctions, where one is a perpendicular connection
   - Case 4, where the source and sensor are separated by two junctions, were both are perpendicular connections
   - Case 5, where the source and sensor are are separated by three junctions and two directional changes.

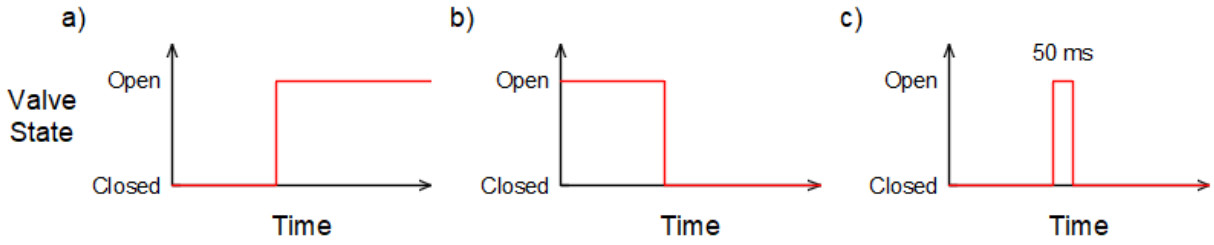

Figure 3.8: Diagram of the solenoid valve state when inducing different transients: a) Closed to Open, b) Open to Closed, c) Pulse.

Table 3.4 shows the overall test matrix used on the two different WDN configurations. Multiple trials were performed for each test case.

Table 3.4: Laboratory test matrix

Parameter	Mode	Original Configuration	Expanded Configuration
Transient Induction Method	Closed to Open	✓	✓
	Open to Closed	✓	✓
	Pulse	✓	✓
Flow Conditions	No Flow	✓	✓
	Flow		✓
Transient Source Location	Case 1		✓
	Case 2	✓	✓
	Case 3		✓
	Case 4		✓

3.2.2 Field experiments

3.2.2.1 Field set-up

The purpose of the field tests is to collect data from a live municipal WDN in order to test the transient detection algorithm. Tests were conducted in DMA 11, a predominantly residential district in the city of Guelph, Ontario that uses 12-inch PVC pipes in its neighbourhood water pipes. For ease of sensor installation, pressure transducers are attached at the ends of modified hydrant stems, and sit within the water column at the base of the selected fire hydrants.

Similar to the laboratory configurations, the tests are conducted in two different neighbourhoods of differing complexity, which are shown in Figure 3.9, where Gosling Gardens is the validation location, and Clairfields is the extended monitoring location.

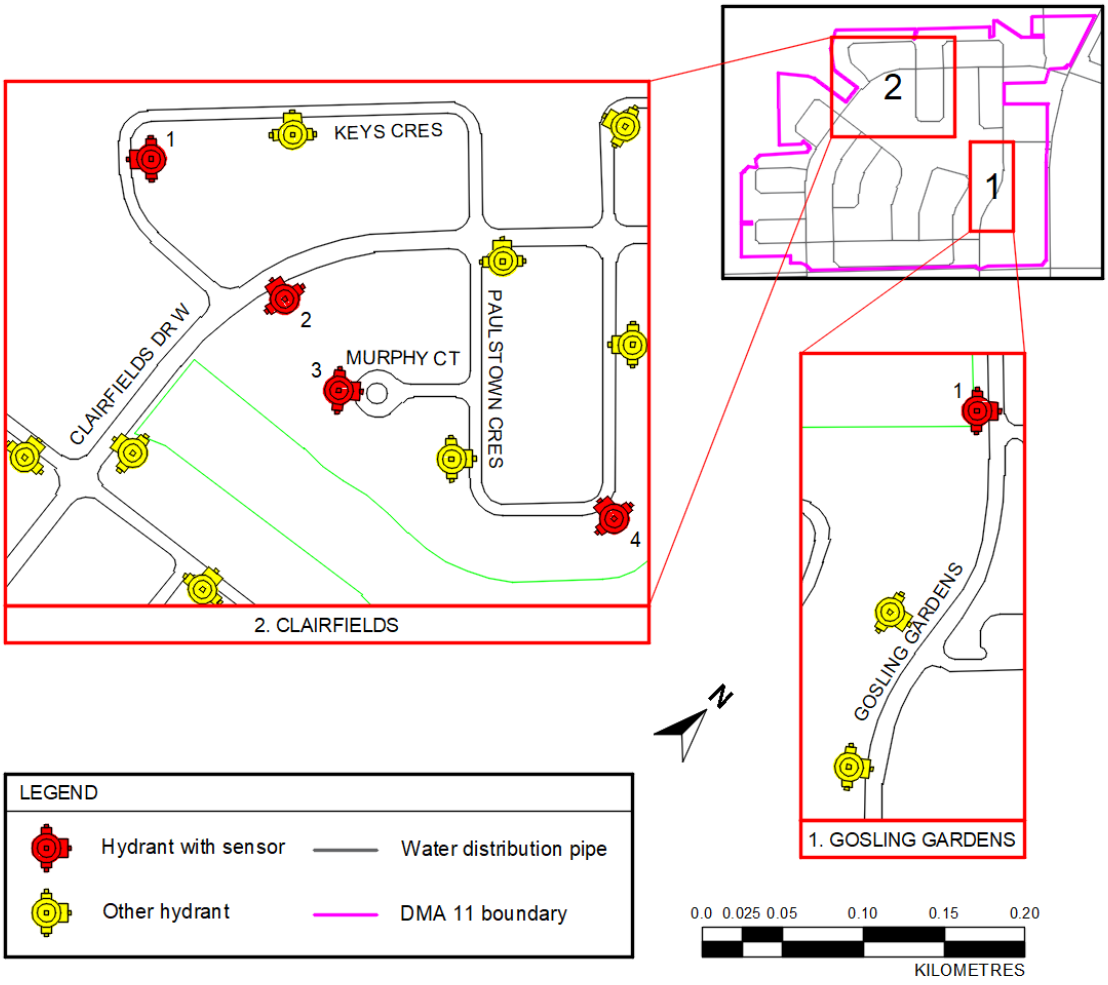

Figure 3.9: Map of field test locations.

3.2.2.2 Field test plan

The Gosling Gardens location is used for algorithm validation, achieved by analyzing its ability to detect known transients induced by flowing nearby hydrants during field tests. The Clairfields location is used to evaluate the system performance in a more complex neighbourhood and to draw conclusions about transient behaviour during regular use. The background continuous monitoring conducted at Clairfields was carried out predominantly in the early morning hours where general demand is reduced, in order for transient events to be more apparent.

The variable parameters are similar to those of the laboratory, but some exceptions

are made due to limitations in the field setting. The main differences are highlighted as follows:

1. For transient induction method, the quick pulses are difficult and possibly dangerous to induce when flowing nearby hydrants, therefore only the controlled opening or closing of a hydrant valve is considered.

2. For flow conditions, the water flow in the field water mains are dependent on general use, are constantly changing, and impractical to control. The only flow setting, therefore, will be the regular, or 'ambient', conditions;

3. Transient source location no longer applies, and instead the focus is on sensor location. Furthermore, the proximity of the sensors to transient sources, especially in continuous background sampling, cannot be anticipated. The sensors are placed throughout the neighbourhood to showcase different network features, including:

    - Case 1, along a major road's water main;
    - Case 2, directly off of a looped residential road's water main; or
    - Case 3, at the end of a residential road's water main.

The overall test plan for both locations is summarized in Table 3.5.

Table 3.5: Field test matrix

Parameter	**Mode**	**Gosling Gardens**	**Clairfields**
Transient Induction Method	Closed to Open	✓	
	Open to Closed	✓	
Sensor Location	Case 1	✓	✓
	Case 2		✓
	Case 3		✓
Flow Conditions	Ambient	✓	✓

Chapter 4

Results

The validation and sensitivity analysis for the proposed transient detection algorithm was performed using the laboratory and field experiments described in the Methodology chapter. The preliminary results for the abnormal transient identification process is also discussed and examined in the current chapter.

4.1 Laboratory results

The laboratory results section examines the findings from the original laboratory configuration, used for validation, and the subsequently expanded configuration which was used for a sensitivity analysis.

4.1.1 Validation - original laboratory configuration

4.1.1.1 Raw and pre-processed data

Data was collected in ten-second samples wherein a transient was induced via solenoid valve by one of the three aforementioned methods. No other flow was generated during the validation tests aside from through the solenoid valve itself. Figure 4.1 shows an example of a raw data set, and one which has undergone the pre-processing detailed in Section 3.1.3.1, taken from the original laboratory configuration in order to illustrate the effect of the first data processing steps. The dominant low-frequency wave is apparent in the raw pressure signal, as is the transient indicated shortly after three seconds have elapsed. The processed

data time series successfully removes the unwanted pressure fluctuations but retains the effects of the transient.

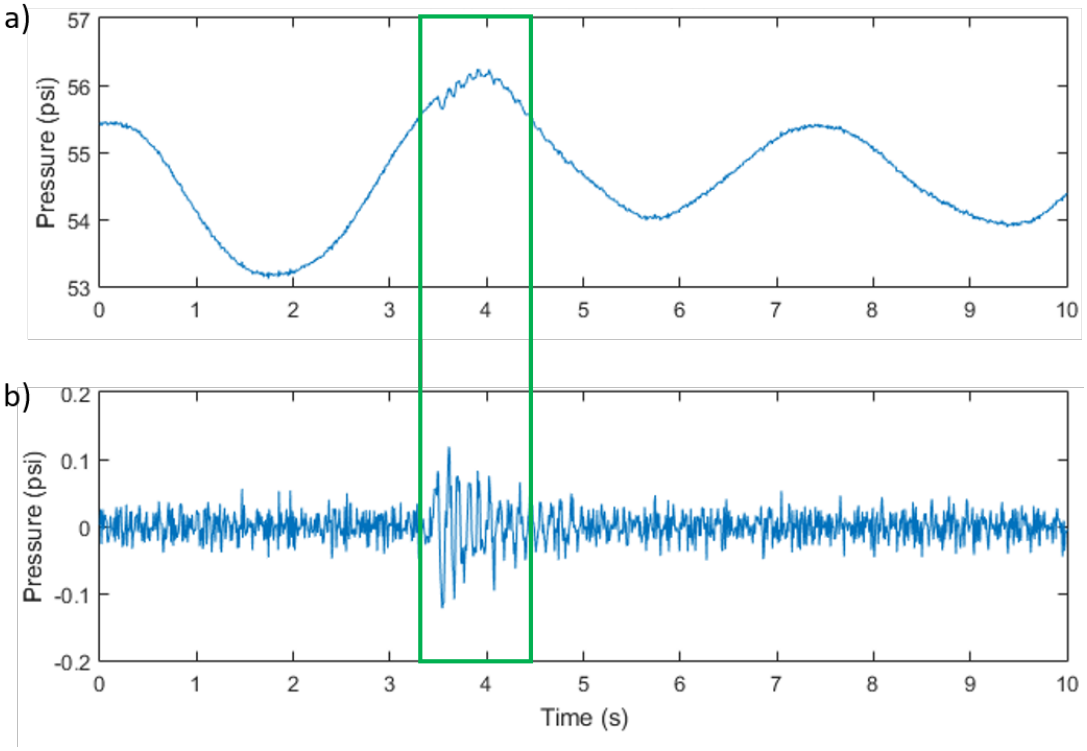

Figure 4.1: Example pressure time series showing a transient occurrence in the original laboratory configuration: a) raw data, b) pre-processed data.

Varying the transient induction method without flow and at a fixed location results in slightly different behaviour in the resulting time series. Figure 4.2 compares the raw and pre-processed data during the indicated transients. In the raw figures, the Closed to Open case shows an initial drop in pressure and the Open to Closed an immediate rise at the occurrence of a transient, which is intuitive given the drop or spike in pressure that occurs when a valve is opened or closed, respectively. Both cases are followed by a short period of transient-related signal oscillation, which is more apparent after pre-processing, before the system returns to equilibrium. The Pulse case, which is effectively a rapid combination of the previous two, shows a pronounced rapid oscillation in the signal following the transient. Comparing the filtered signals, the behaviour and amplitude of the transient in the Open to Closed case is similar to the Closed to Open case, while the Pulse case exhibits a more prolonged oscillatory response and a slightly larger amplitude than the other two cases.

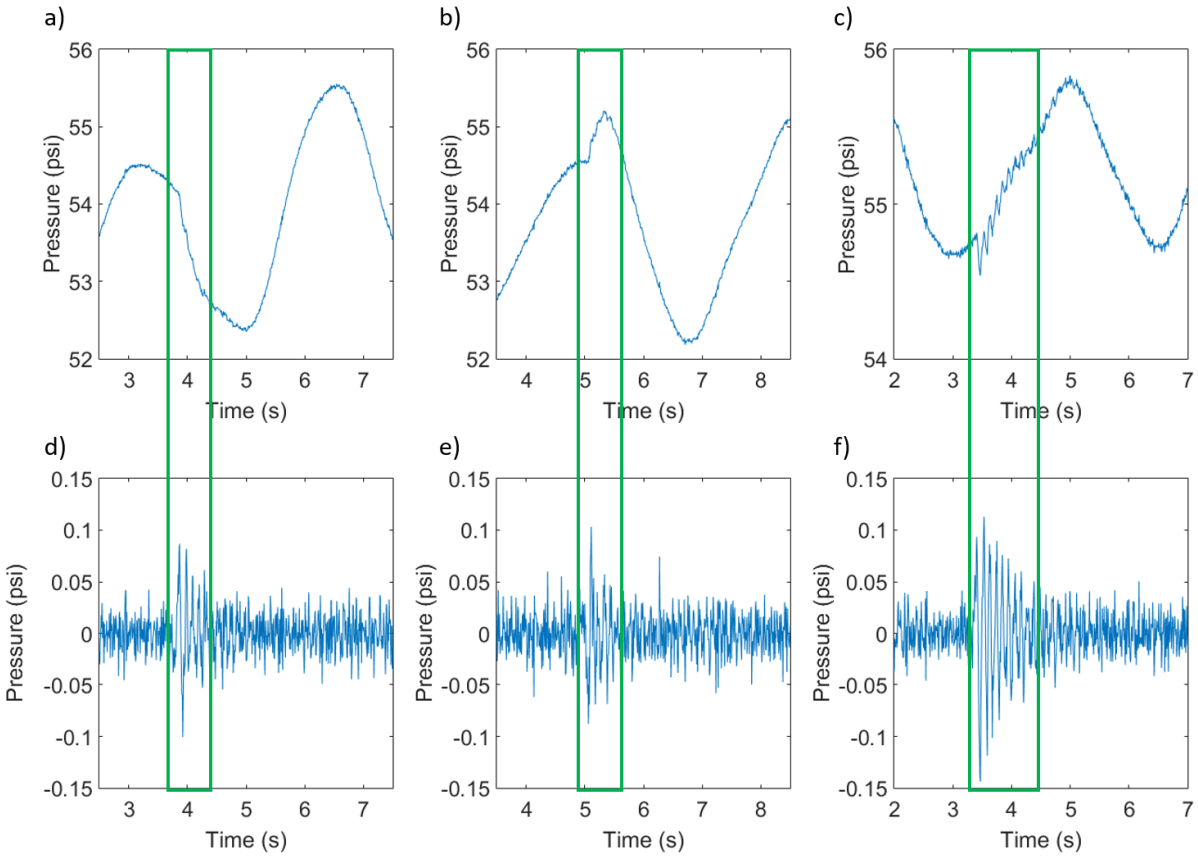

Figure 4.2: Example pressure time series showing a transient occurrence in the original laboratory configuration for the three transient induction methods. Raw: a) Closed to Open, b) Open to Closed, c) Pulse; Pre-processed: d) Closed to Open, e) Open to Closed, f) Pulse.

4.1.1.2 Performance of anomaly detection algorithm

After undergoing the data pre-processing and feature classification modules, the ultimate identification of an anomaly relies heavily upon a majority voting method, which counts the number of features that experienced exceedances within each time interval. Setting an appropriate threshold for the number of votes is important for the overall accuracy of the algorithm.

In order to optimize the voting threshold, its effect on the detection and error rates was evaluated for each transient induction method, which is visually illustrated in Figure 4.3. The detection rate is considered to be the percentage of times when a known transient was classified as such by the algorithm, which should be maximized by the threshold. An

appropriate threshold would also aim to minimize the error rate, comprised predominantly of false positives (or Type I errors), while maximizing the rate of successful transient identifications. In this case, *false positives* refer to instances where a number of features were triggered, but there was no expected or visually discernible transient. It's important to note that in some of these cases, there may in fact be a transient-like fluctuation in pressure. However, the effect of these fluctuations is very small, especially when considering that the size of the solenoid valve itself is very small compared to other potential transient sources in a network.

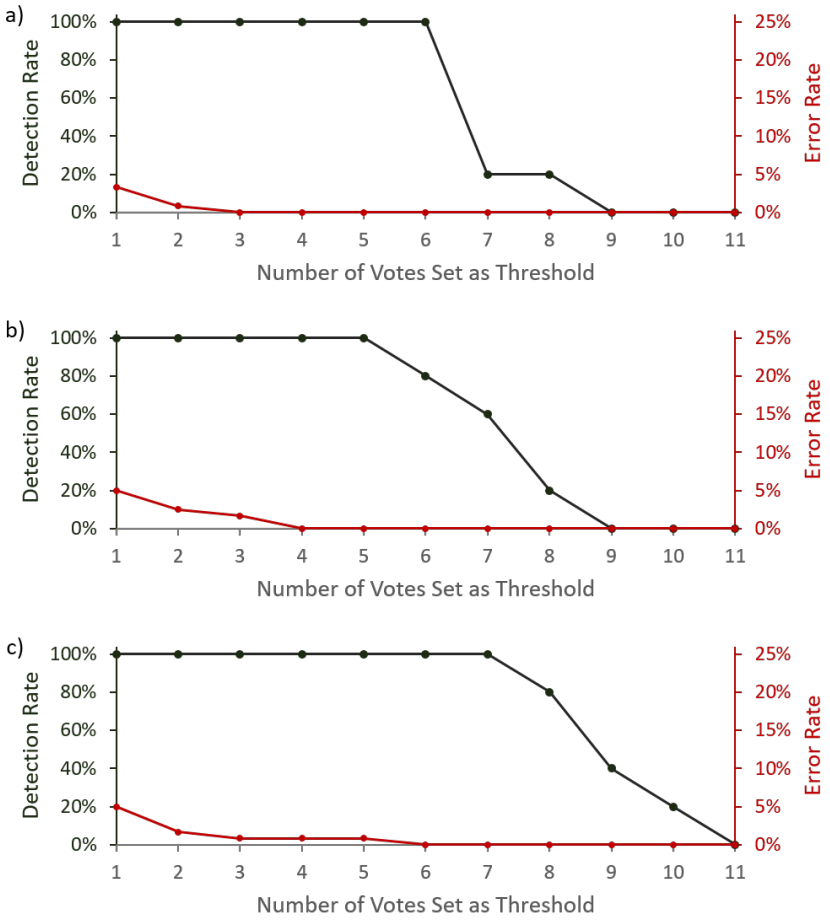

Figure 4.3: Detection and error rates when using each feature vote threshold in the original laboratory configuration for the three transient induction methods: a) Closed to Open, b) Open to Closed, c) Pulse.

Based on the validation tests, the detection rate is most accurate when set below 6, while the error rate is reduced when using thresholds above 3 or 4, although even the

highest error rate here can still maintain a confidence of 95%. The voting threshold can be further analyzed using the test data from the expanded configuration, but the original configuration tests show that the algorithm is successful identifying pressure transients with a high degree of accuracy, while maintaining a low rate of errors due to false positives.

4.1.2 Sensitivity analysis - expanded laboratory configuration

With the added complexity provided by the expanded configuration, new elements were discovered in the pressure signals that affected the algorithm performance. In some cases, secondary transients, caused by reflections within the system, could be detected. The occurrence of these smaller transients typically triggered fewer feature exceedances and were not as visually discernible, as shown in Figure 4.4.

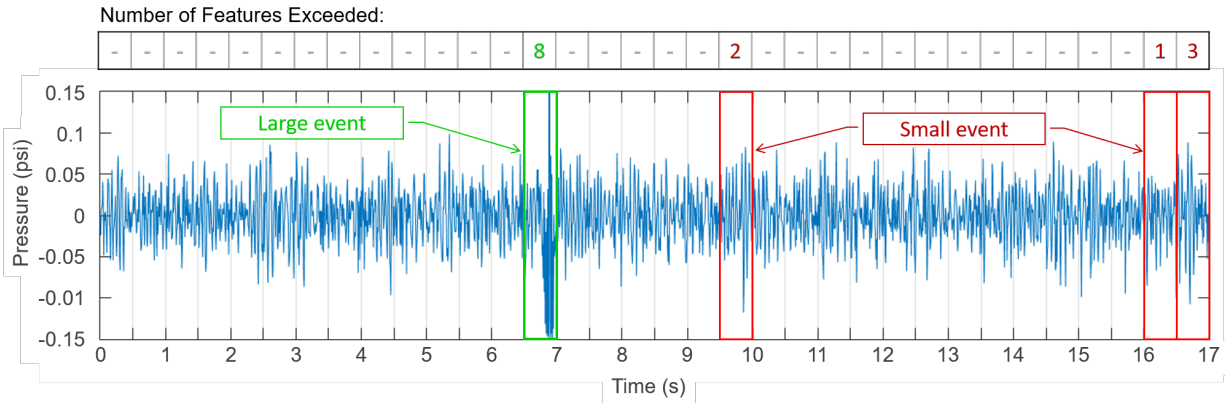

Figure 4.4: Example pressure time series showing different transient occurrences in the expanded laboratory configuration with their corresponding feature vote.

Another element introduced by the expanded set-up is the occurrence of *false negatives*, where the algorithm failed to identify a known event, typically resulting from transient dissipation in the more complex network. The false negative can therefore be considered, by definition, to be the complement of the detection rate. The false negatives (or Type II errors) contribute to a slightly increased overall error rate across the thresholds.

Sensitivity analyses performed on the expanded laboratory configuration allow for a more precise optimization of the voting threshold. The optimization of the voting threshold would depend on the objective of a given study. For example, the threshold could be set higher when attempting to predict pipe failure, where the only transients of interest are large ones. Contrarily, the threshold may be set lower if the purpose is to assess

long-term pipe stress from water use and demand, in order to include smaller, frequently-occurring transients. The assessment of algorithm performance can be further improved with the consideration of additional test parameters such as the effect of flow conditions and transient source location.

4.1.2.1 Transient induction method

Similar to tests done in the original configuration, three types of transients were induced in order to represent different activities that would cause transients, and example pressure time traces can be seen in Figure 4.5. Unlike in the original configuration, the behavioural nuances and the differences in behaviour between the three methods could not be visually discerned as easily, in either the raw or pre-processed data. However, the pressure spikes resulting from the Pulse method were generally greater in amplitude than the other cases.

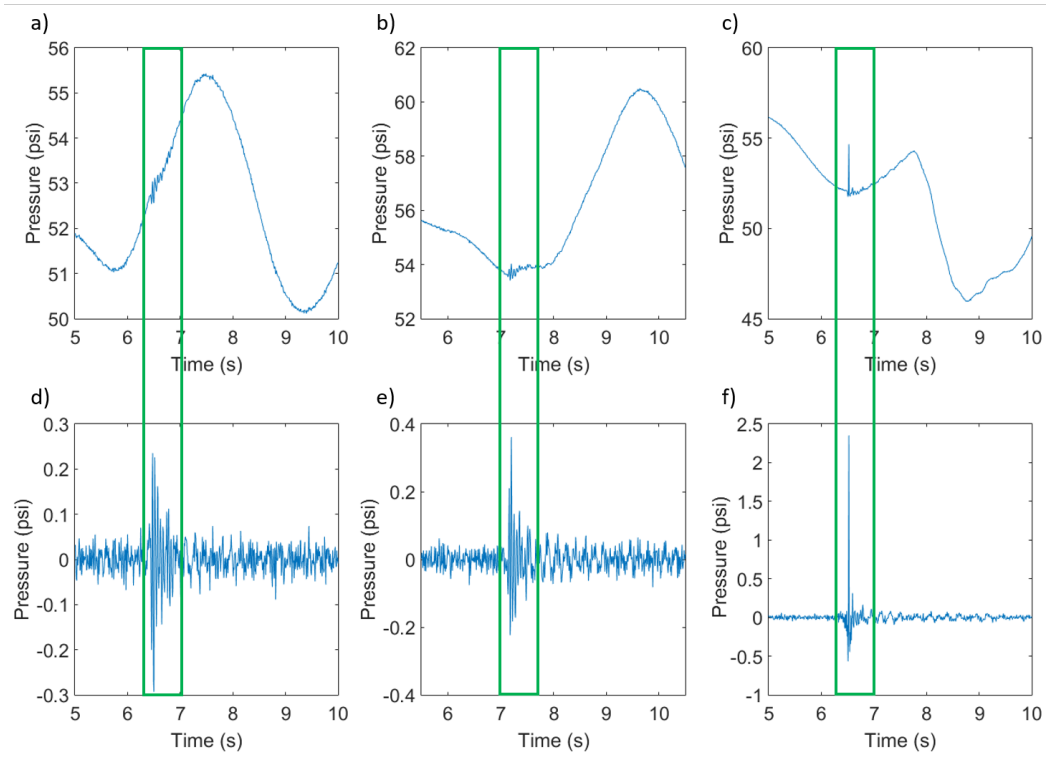

Figure 4.5: Example pressure time series showing a transient occurrence in the expanded laboratory configuration for the three transient induction methods. Raw: a) Closed to Open, b) Open to Closed, c) Pulse; Pre-processed: d) Closed to Open, e) Open to Closed, f) Pulse.

The algorithm's ability to identify the three transient types across different voting threshold settings is illustrated in Figure 4.6. The detection rates were highest for the Pulse, where the error rates were also the lowest. The comparisons also support the idea that the Pulse was the easiest to detect, followed by Open to Closed and then Closed to Open.

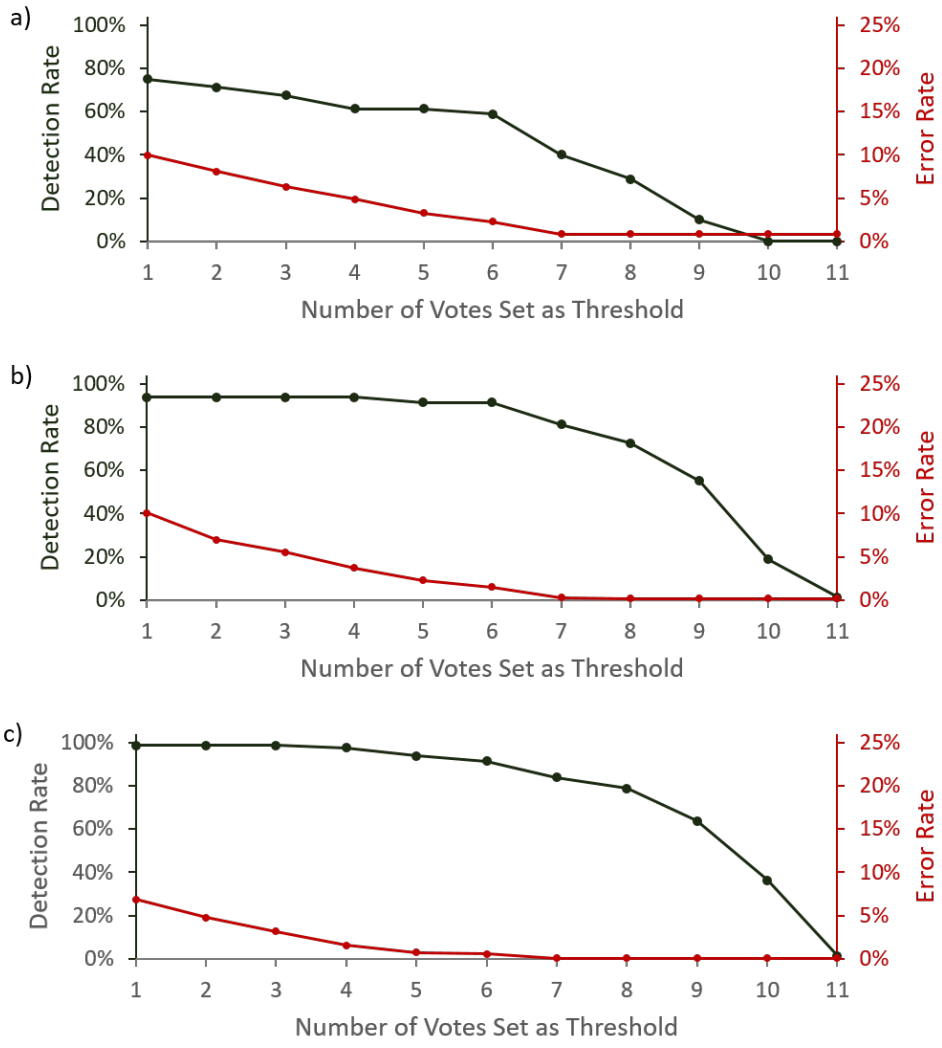

Figure 4.6: Detection and error rates when using each feature vote threshold in the expanded laboratory configuration for the three transient induction methods: a) Closed to Open, b) Open to Closed, c) Pulse.

For all three cases, the detection rate was high below a threshold of approximately 6, after which the percentage detected decreased more dramatically. However, in terms of

errors, a threshold above 7 was found to be ideal for minimizing the error rate. Given these circumstances, the range for the optimal threshold would be rather narrow, but it may be noted that even with the addition of the false negatives to the error, the highest error rates still did not exceed 4%, indicating that the slightly lower thresholds may still be ideal.

4.1.2.2 Flow conditions

The second parameter tested was flow conditions, where the presence of flow was added by opening the two outlet valves in the system previously illustrated in Figure 3.6. The addition of the Flow conditions also caused an overall decrease in network pressure of approximately 35 psi compared to No Flow conditions. Figure 4.7 shows an example of a raw and pre-processed time series with an induced transient for the two different background condition cases. Generally, the non-transient parts of the signal for the Flow case were noisier and exhibited a relatively higher energy. However, the reduced pressure can also reduce the severity of the transients experienced by the system.

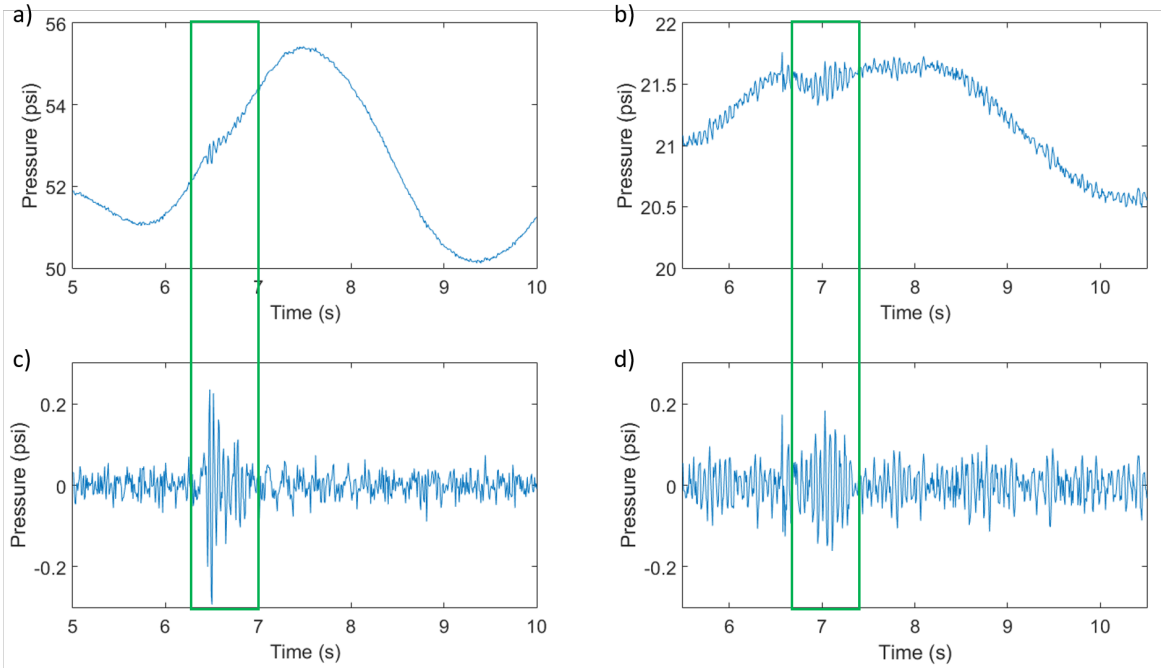

Figure 4.7: Example pressure time series showing a transient occurrence in the expanded laboratory configuration for the two flow conditions. Raw: a) No Flow, b) Flow; Pre-processed: c) No Flow, d) Flow.

The ability for the algorithm to detect transients within both scenarios is shown in Figure 4.8. The added noise in the Flow case results in an approximately 10% drop in detection rate across the thresholds. Additionally, the presence of flowing water also greatly increased the likelihood of error because it added pressure phenomena that were more easily misidentified as meaningful transients by the algorithm. The No Flow case showed that a threshold below 6 would maximize its detection rate, and that virtually any threshold at all would minimize the error rate. The Flow case was less forgiving in that the detection rate is relatively low overall, however there is little loss in detection rate until a threshold of 6, while the error can be kept below 5% above a threshold of 5.

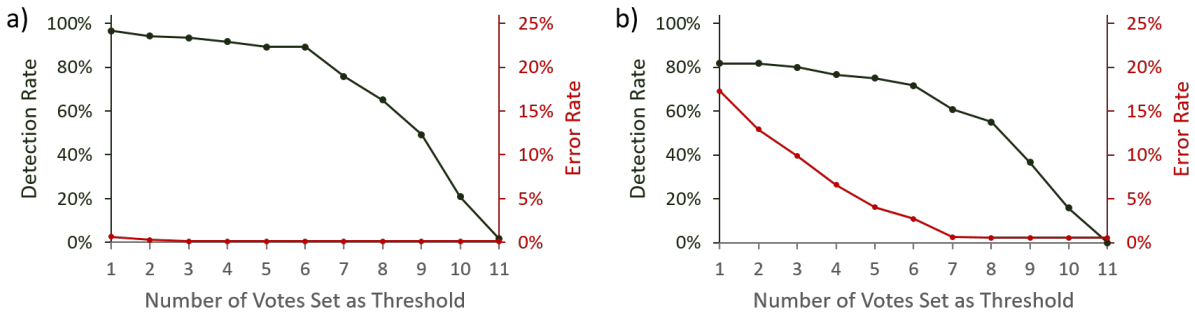

Figure 4.8: Detection and error rates when using each feature vote threshold in the expanded laboratory configuration for the two flow conditions: a) No Flow, b) Flow.

4.1.2.3 Transient source location

The last main parameter that was varied in the sensitivity analysis was the location of the transient source, which in this case is the position of the solenoid valve. The effect of distance and level of complexity between the sensor and the source can affect algorithm performance. The complexity increased across the cases, with Case 1 being the simplest and Case 4 being the most complex. For the purpose of the discussion, Solenoid 1 is placed at the Case 1 location, Solenoid 2 at Case 2, and so forth. Each location has some important factors to note which may affect transient propagation. Solenoids 1 and 4 are positioned along straight sections of pipe and are relatively further from network features such as junctions and dead ends, while Solenoids 2 and 3 are positioned in close proximity to a junction and a dead end, respectively. Figure 4.9 shows example time traces from the four chosen locations. From only these plots, the transient seen from Solenoid 1 had a slightly larger amplitude than the others, while Solenoid 2 had the smallest.

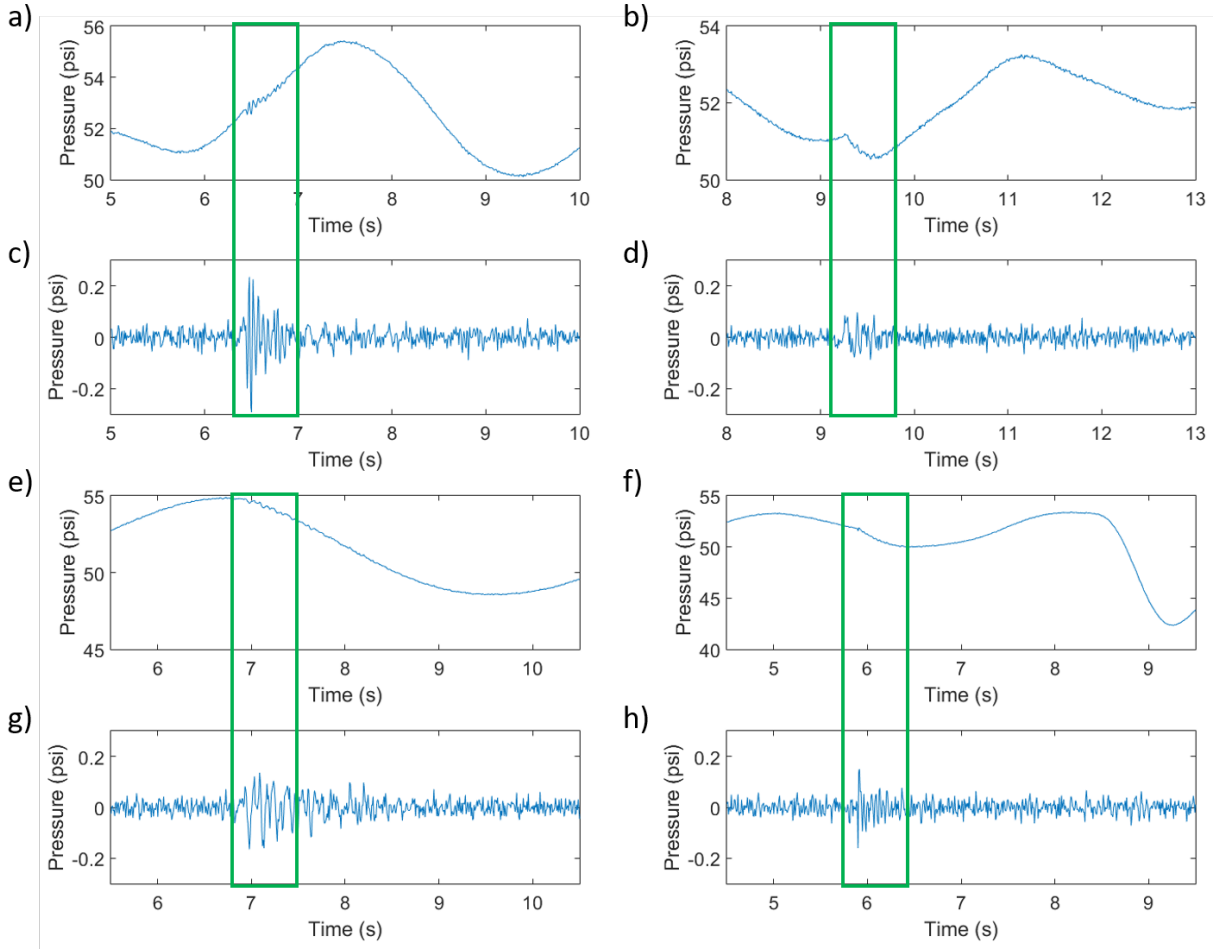

Figure 4.9: Example pressure time series showing a transient occurrence in the expanded laboratory configuration for the four transient source locations. Raw: a) Solenoid 1, b) Solenoid 2, e) Solenoid 3, f) Solenoid 4; Pre-processed: c) Solenoid 1, d) Solenoid 2, g) Solenoid, h) Solenoid.

It is difficult to draw immediate conclusions from the raw signals, so the detection and error rates across the potential threshold values are shown in Figure 4.10, from which many conclusions can be drawn. Firstly, the detection rates for transients sourced from Solenoids 1 and 4 were, on average, 10% higher than those from 2 and 3. This suggests that the ability for a transient to travel is significantly affected by the nearby presence of a network feature. Transients that immediately strike a junction or dead end will dissipate faster than those who begin along straight pipe sections, and will be harder to detect at a further location in the network. The error rates for Solenoids 2 and 3 were very small, and Solenoid 4 only exceeded 5% at the lowest threshold of 1. However, the large error

rate from Solenoid 1 indicates the presence of a large number of transient-like behaviours stemming from the reflections and disruptions caused by the nearby features, which were identified by the algorithm but would otherwise be negligible in most studies. It can be inferred that the sensor nodes should not be placed too close to a suspected transient source. Generally, the detection rates experienced a pronounced decline after a threshold of 6, while the error rates tended to be minimized around 2 to 6.

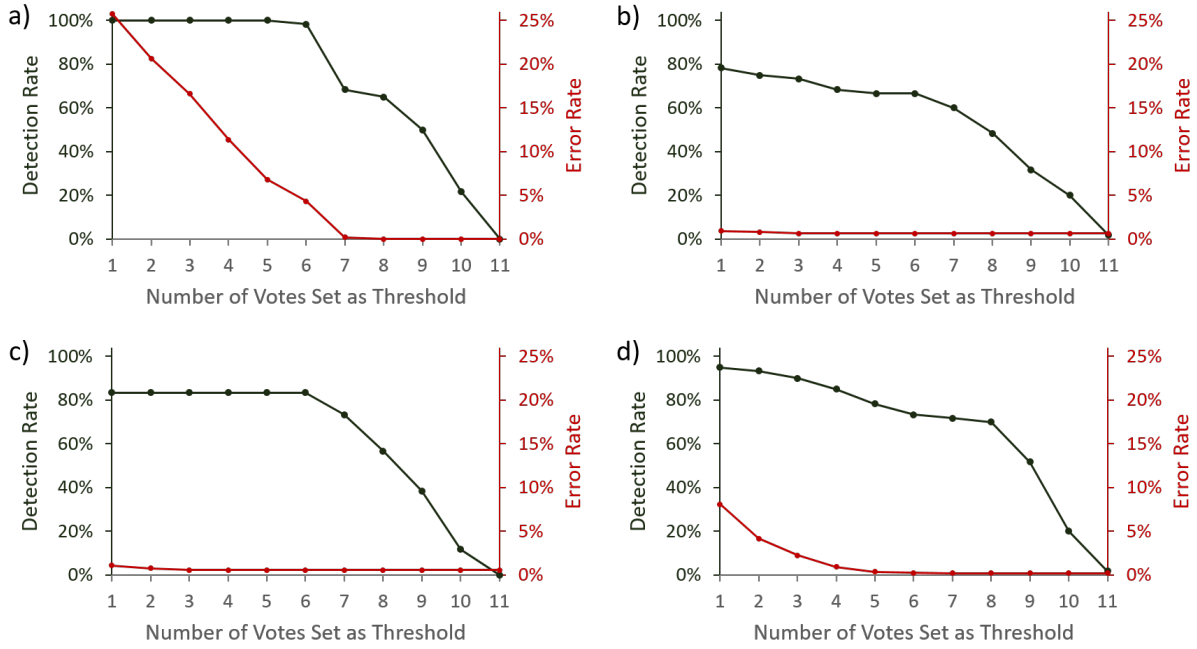

Figure 4.10: Detection and error rates when using each feature vote threshold in the expanded laboratory configuration for the four transient source locations: a) Solenoid 1, b) Solenoid 2, c) Solenoid 3, d) Solenoid 4.

4.1.2.4 Summary of the sensitivity analysis

While some cases resulted in higher accuracy of transient identification than others, the detection and error rate curves for all cases exhibited similar tendencies. Averaging all the data sets across the different analyses, a general quantification of the detection and error rates using various voting thresholds can be obtained. Figure 4.11 shows the resulting plot, which reflects the trends previously seen throughout the sensitivity analysis. A detection rate above 85% can be maintained until a threshold of 3, and can be maintained above 80% until 6, after which the detection rate begins a considerable decline. The error rates

are consistently low, never over 10%. A voting threshold above 3 can be used to achieve a rate below 5%, while choosing a threshold above 6 will reduce that to near 1% while still maintaining a reasonable detection rate.

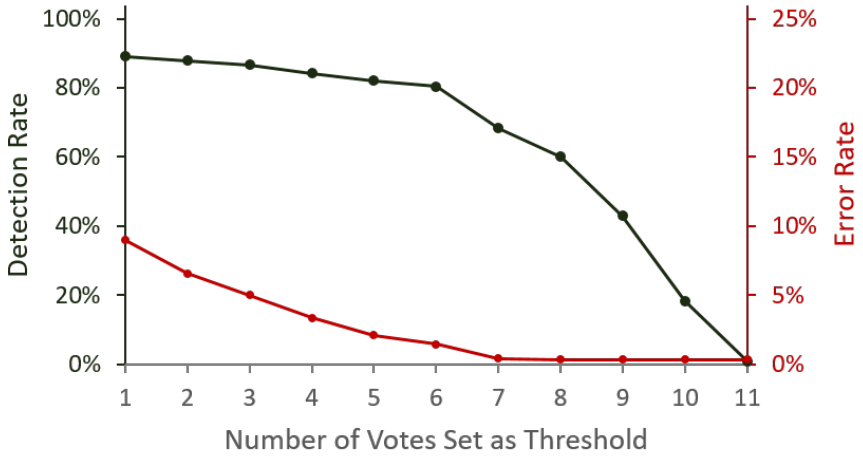

Figure 4.11: Overall detection and error rates by feature vote threshold.

When considering field implementation, the purpose of the monitoring would help to determine the optimal voting threshold to use, but based on the laboratory tests the ideal range is between 3 and 7, depending on whether or not less severe transients are deemed important for inclusion in the given test.

The results from the analysis can be used to derive probability distributions based on the thresholds, as shown in Figures 4.12 and 4.13. This way of representing data can be used to further investigate the effect of the individual threshold levels in identifying pressure transients. Figure 4.12 therefore reveals that 9 features were triggered in nearly 30% of the identified transients, and that using a thresholds above 7 would account for 77% of the identified transients.

If the aim is to minimize false alarms, perhaps it is more appropriate to look at the breakdown of the error rates. Similar to the detection rates, thresholds between 8 and 10 were the safest to use when assessing the likelihood that a real transient has occurred. In fact, based on the laboratory data, if the system has identified a transient in which 8 to 10 features were triggered, there is a 0% chance that the identification was an error. That is, it is definitive that a transient occurred, that it is very likely that that transient resulted in a significant pressure change.

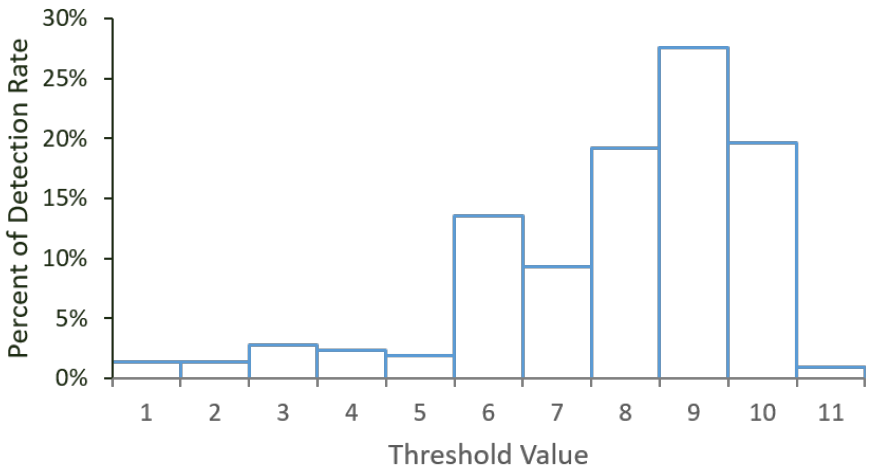

Figure 4.12: Detection rate at each individual feature vote.

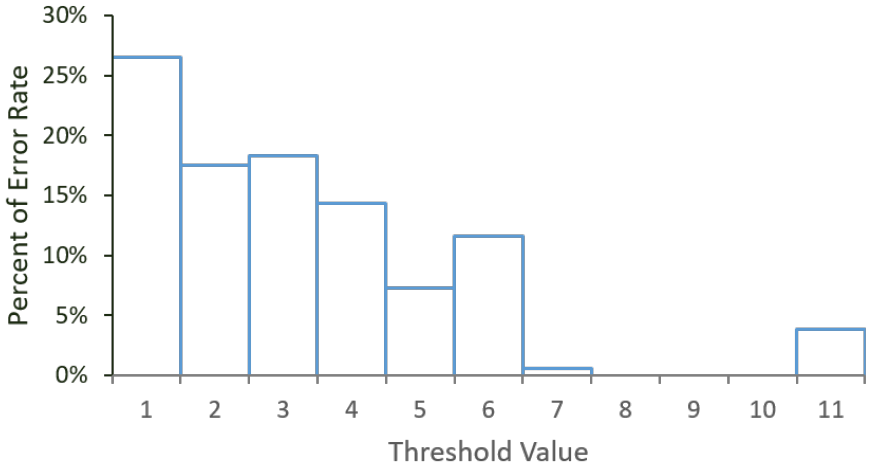

Figure 4.13: Error rate at each individual feature vote.

4.1.3 Additional analysis for abnormal transient detection

Generating transients that could be classified as abnormal was impractical and difficult, and in the case of severe transients, dangerous. Consequently, the second-tier SPC process for the detection and ranking of abnormal transients could not be completely validated. However, analysis was nonetheless conducted in order to illustrate the concept and determine the most suitable features to be used.

Being that the transient data used in the second process must first be identified by

the initial SPC process, the first tier results from the laboratory sensitivity analyses can now be used towards creating the training data for the future identification of abnormal transients. The data sets corresponding to transient events for each feature were evaluated for their normality, or ability to be transformed to follow a normal distribution. For the case of the laboratory data, the best example of a naturally normally distributed feature data set was the Zero-Crossings Count, as shown in Figure 4.14.

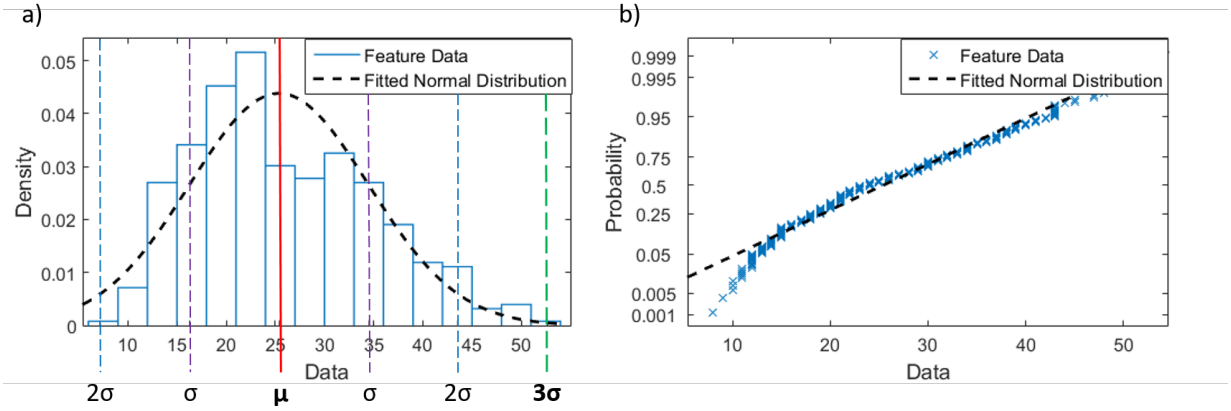

Figure 4.14: a) Probability distribution, and b) probability paper plot of laboratory transient Zero-Crossings Count data.

The Maximum feature provides an example of a data set that did not initially conform to a normal distribution but was successfully transformed to do so using a Box-Cox Transformation, which is exemplified in Figures 4.15 and 4.16.

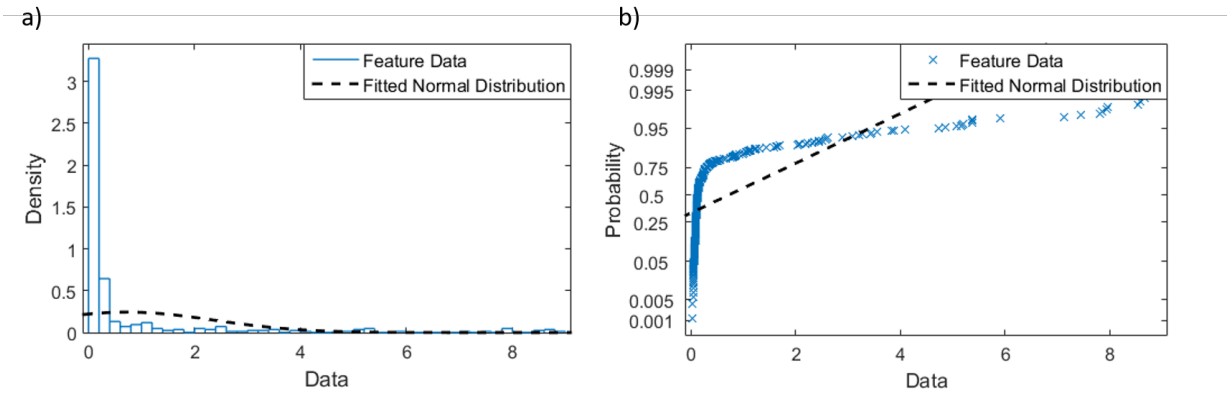

Figure 4.15: a) Probability distribution, and b) probability paper plot of laboratory transient Maximum data.

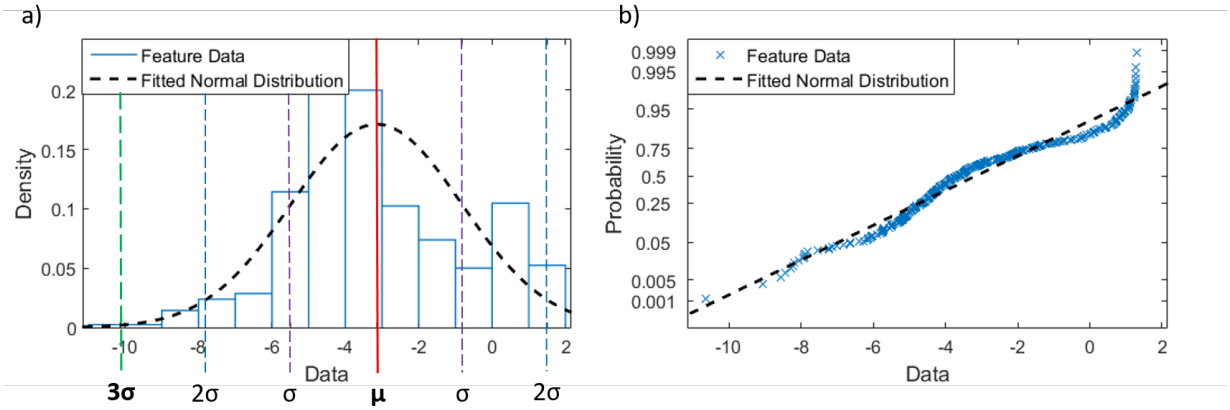

Figure 4.16: a) Probability distribution, and b) probability paper plot of Box-Cox transformed laboratory transient Maximum data.

Table 4.1 details the features that were found to be most efficient for the SPC process, with notes on whether a Box-Cox transformation was needed to achieve normality. Seven of the eleven original features were deemed suitable for use (i.e. exhibited a normal distribution).

Table 4.1: Abnormal transient detection feature set for the laboratory

Feature	**Normal**	**Transformed**
Maximum		✓
Minimum		✓
Root-mean-square		✓
Zero-crossings count	✓	N/A
Energy		✓
Cumulative Sum (Upper)		✓
Cumulative Sum (Lower)		✓

Of the omitted features, Kurtosis and Entropy could not approach a normal distribution even with the use of a transform, while the Mean and Skewness both had distributions

that resembled normal but their variances were too small and large, respectively, which affected their uniformity when using probability paper plots for confirmation.

Despite the lack of abnormal transient data with which the method can be validated, the distributions generated using the sensitivity analysis can allow for the deduction of some results. There was no significant number (i.e. less than 0.3%) of transients that exceeded the three-sigma bounds of any of the pertinent features, as would be expected because no high-risk transients were experienced during testing. Hence, it is reasonable to assume that any transient exhibiting feature values outside of these three sigma thresholds can be considered abnormal and potentially dangerous.

4.2 Field results

The primary purpose of the field trials is to assess the applicability of the algorithm to real-life situations. The results of the assessment is summarized in the following section.

4.2.1 Validation - Gosling Gardens

The Gosling Gardens field setup is a simple setup consisting of a linear water main following a more major residential road, as shown in Figure 4.17.

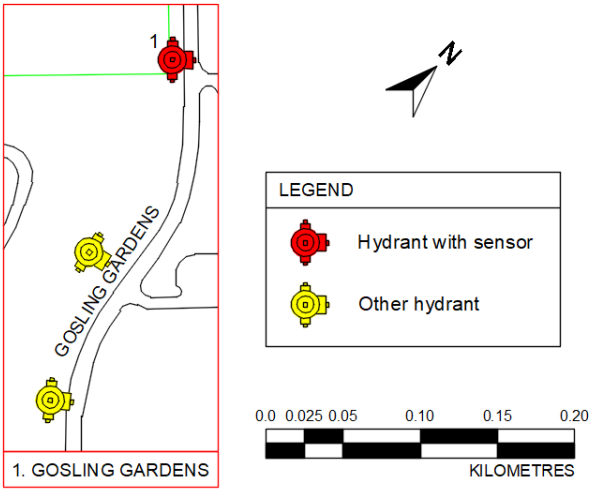

Figure 4.17: Map of Gosling Gardens test location.

Pressure data was collected from sensors fitted onto the end of a modified hydrant stem, similar to that shown in Figure 4.18. Transients were induced by opening or closing a valve connected to a neighbouring fire hydrant, illustrated in Figure 4.19. Between the sensor and the transient source, there is only one primary junction that connects to another section of water main, and the various junctions that lead to individual residential service lines are significantly smaller.

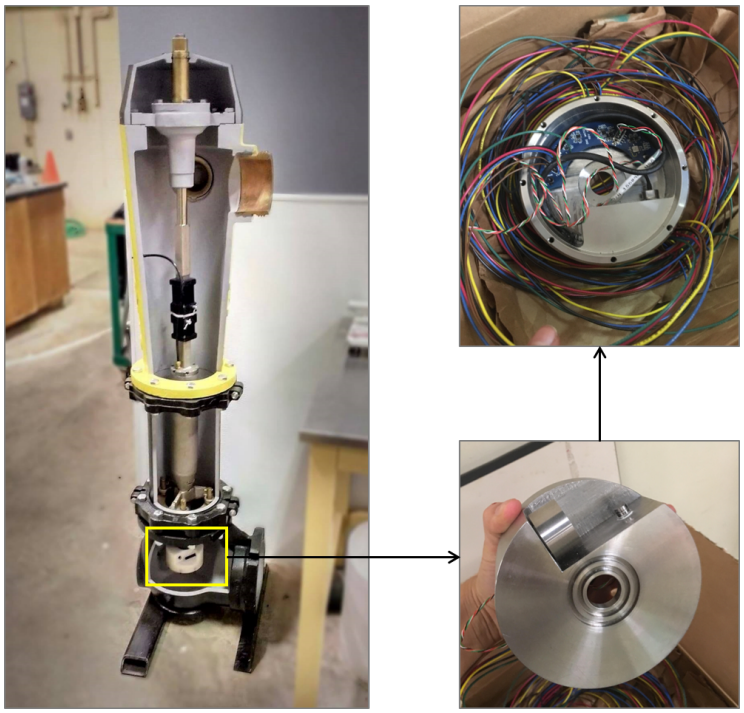

Figure 4.18: Sensor placement within a fire hydrant.

Figure 4.19: Water flowing from a hydrant port valve during field tests.

Figure 4.20 shows an example of the pressure signal from a flow test, consisting of five minutes of data, in which three transients were induced. The first transient resulted from initial tests with the valve, the second resulted from the valve opening and the last from the valve closing. The algorithm successfully identified all three instances, as well as a number of smaller transient occurrences. In this particular case, setting a threshold of 4 would allow for the identification of all the induced transients while ignoring the smaller events. Setting a threshold of 3 would account for all phenomena picked up by the algorithm.

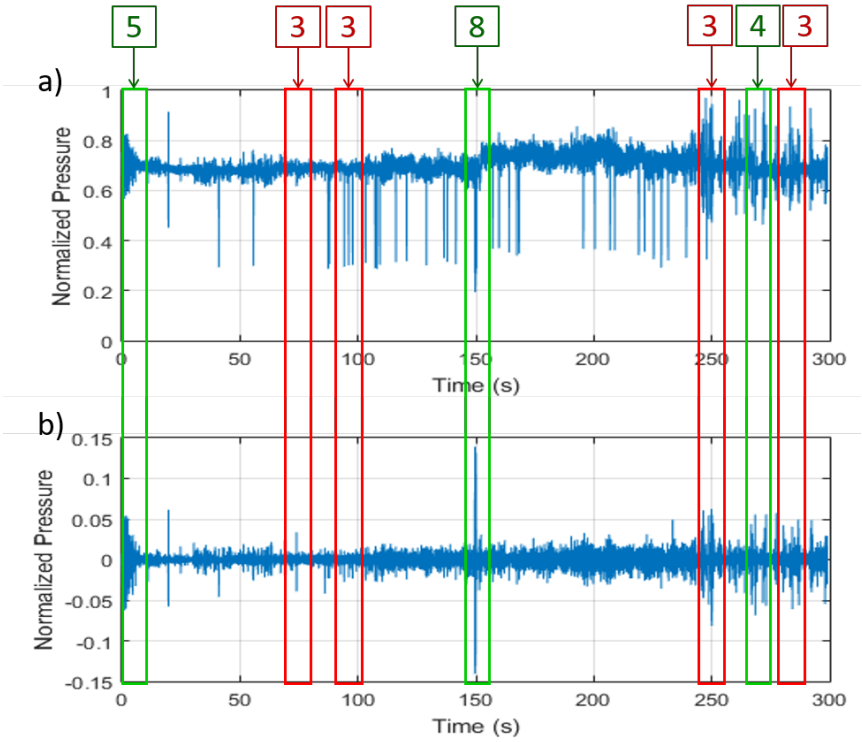

Figure 4.20: Example pressure time series showing transient occurrences in the Gosling Gardens field location: a) raw data, b) pre-processed data.

The algorithm has been shown to have the capacity to correctly identify transient events in a real municipal WDN, while demonstrating the need to calibrate the threshold to be more appropriate for different needs.

4.2.2 Detailed analysis - Clairfields

The Clairfields location included four sensor locations placed in a neighbourhood with a more complex layout, which is analogous to the expanded setup in the laboratory. The

locations are illustrated in Figure 4.21. The four locations were chosen to represent various features within a WDN, in order to study how pressure transients might affect them differently. It is important to note that, since fire hydrants are typically connected to a water main by individual valved pipes, all the sensors are technically placed at dead ends. Flow tests were not conducted, and the focus was instead placed on deploying the system to conduct continuous background monitoring.

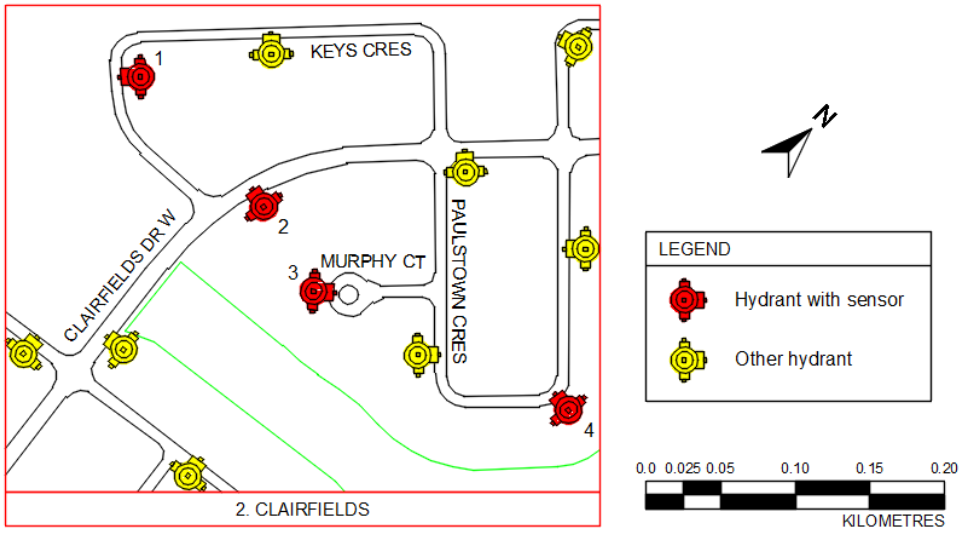

Figure 4.21: Map of Clairfields test location.

The results to be displayed were taken from a time period between 2:00 a.m. and 8:00 a.m., averaged from data aggregated during the second week of November, 2018. The examination of early morning data helps to reduce the effect of pressure fluctuations caused by external factors and network noise, in turn helping to achieve a more accurate transient count. Based on validation tests, two thresholds, 3 and 7, were chosen for comparison as they had both been shown to be optimal for different monitoring objectives.

4.2.2.1 Location 1 - 38 Keys

The first sensor location is an example of a Case 2 placement type, since it is located near a gentle bend along a water main following a relatively small road, and otherwise far from prominent network features. Figure 4.22 shows, for each half-hour increment during the time of study, the rate at which the transients were being identified per minute.

Based on the results, there was relatively little activity throughout the test period,

and no discernible patterns. A threshold of 3 yielded an average transient rate of 0.65 transients/minute, or around 20 transients in each half-hour block. A threshold of 7 allowed for the identification of very few large transients, averaging at 0.08 during the study, which can be interpreted as being around two larger transients per half-hour time interval.

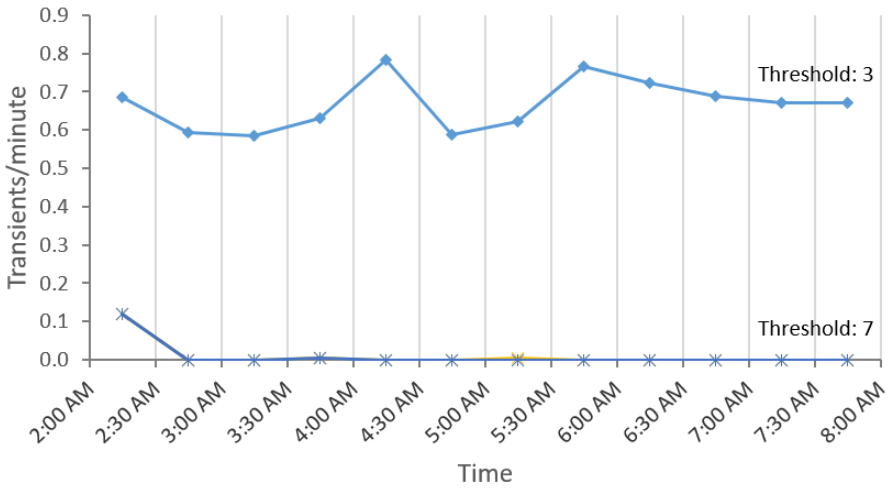

Figure 4.22: Number of transients identified per minute using feature vote thresholds 3 & 7 during early morning hours at 38 Keys.

4.2.2.2 Location 2 - 70 Clairfields

The second location at 70 Clairfields Drive West, experienced the largest number of transients according to the identification system. As a Case 1 placement, the sensor is located along a primary water main which services the smaller residential streets. As a result, it is not only affected by the water demands from a wider area, but it is also more susceptible to pressure fluctuations resulting from operational equipment and changes both within and outside the DMA.

Figure 4.23 shows that at its peak during the 5:00 a.m. to 5:30 a.m. time frame, the threshold of 3 identified transients at a rate of 35 transients/minute, and the 7 threshold identified 4 transients/minute. Counter-intuitively, both curves exhibited trends opposite to the expected water demand, where the transient identification rate increased dramatically towards 4:30 a.m. and decreased after 5:30 a.m. It is possible that as its a primary supply line, operational equipment such as pumping stations may have increased activity during that time in order to prepare for the expected morning increase in demand.

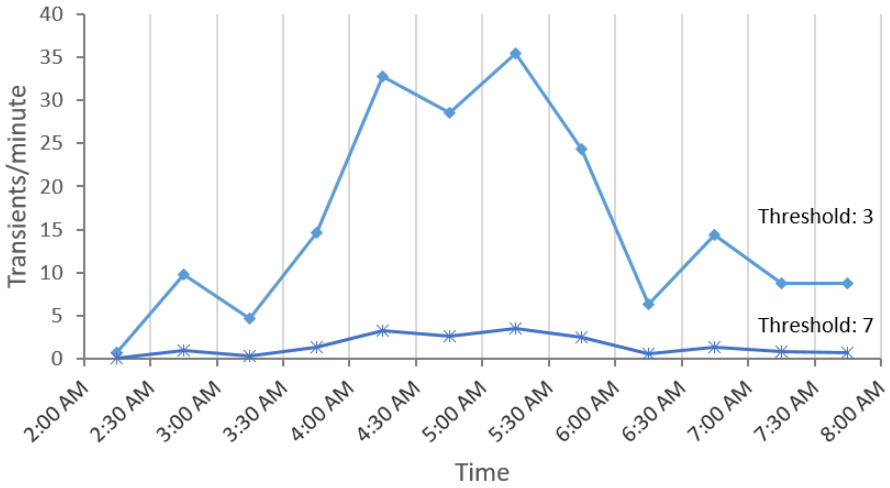

Figure 4.23: Number of transients identified per minute using feature vote thresholds 3 & 7 during early morning hours at 70 Clairfields.

4.2.2.3 Location 3 - 10 Murphy

Location 3, at 10 Murphy Court, also experienced a substantially higher rate of transients, though it was less than the frequency in Location 2. Unlike the 70 Clairfields location, the trends in the morning transient activity mirrored the expected water demand for the morning time period, as seen in Figure 4.24.

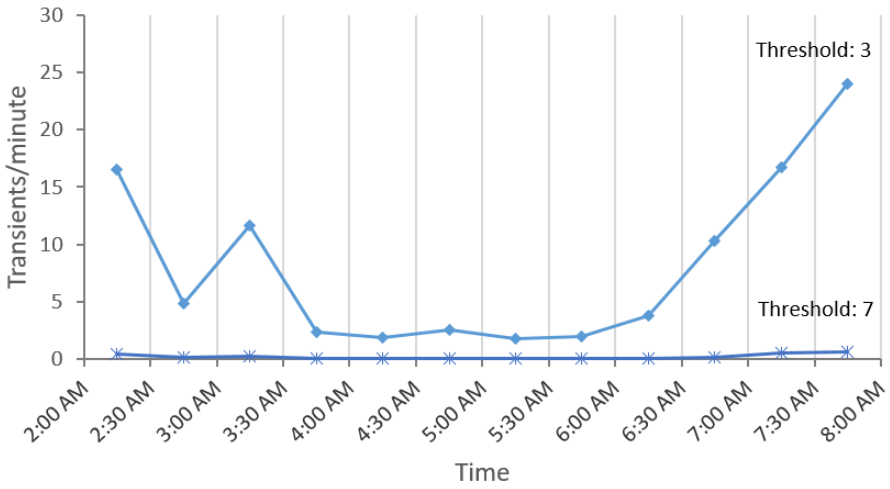

Figure 4.24: Number of transients identified per minute using feature vote thresholds 3 & 7 during early morning hours at 10 Murphy.

Located at the very end of the court, which is a Case 3 placement type, the sensor location might have experienced elevated transient activity due to the transient reflections occurring in its vicinity. Figure 4.24 shows that the threshold of 3 resulted in rates between 3 to 24 transients/minute, while the threshold of 7 reflected approximately one transient/minute. Both curves showed a marked decline in transient-inducing activity towards 4:00 a.m., increasing again between 6:30 to 8:00 a.m.

4.2.2.4 Location 4 - 30 Paulstown

The last location is at 30 Paulstown Crescent and experienced similar transient behaviour to the first location, which also has a Case 2 placement on a crescent. For both Location 1 and 4, it is possible that their location away from WDN junctions and dead ends caused the sensors to detect transients that would have mostly dissipated before reaching the hydrant location. Furthermore, the sensors are both placed relatively far from the major road's water main, limiting their nearby transient sources to purely residential use.

Figure 4.25 shows that there wasn't a dramatic trend in transient identification using either threshold, although a very slight increase can be seen towards the 4:00 to 4:30 a.m. time interval. Using a voting threshold of 3 resulted in an average of one transient identified per minute, and using 7 was about half that.

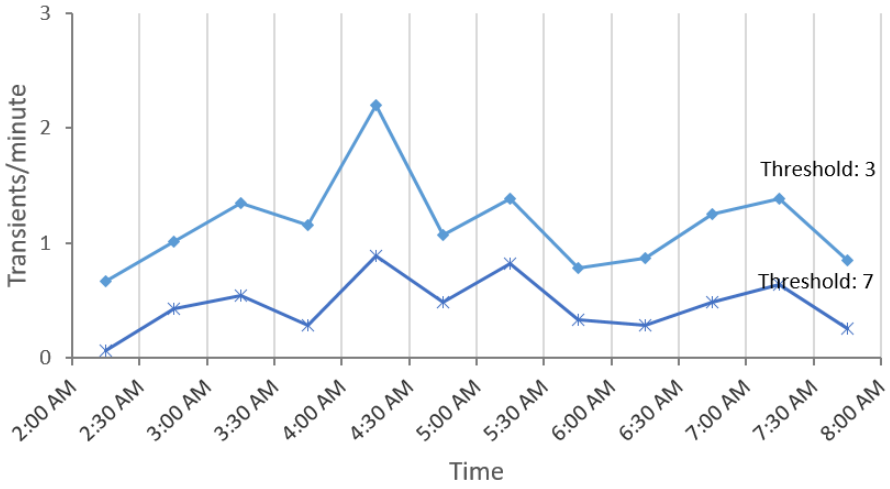

Figure 4.25: Number of transients identified per minute using feature vote thresholds 3 & 7 during early morning hours at 30 Paulstown.

4.2.3 Field application of abnormal transient detection algorithm

The second-tier SPC process was applied to the Clairfields field data. Following the same methodology used for the laboratory data, the analysis began by building feature probability distributions from a training set containing all transients identified with any threshold above zero. The resulting feature probability distributions varied by location. With the exception of the 38 Keys location, which experienced far fewer transient events, the majority of the feature probability distributions from the remaining locations were found to be normally distributed. This result was contradictory to the skewed distributions of the laboratory feature set. The differences in the resulting probability distributions can be attributed to the different constitutions of the training sets. In the laboratory, the training data consisted solely of induced transient events, which are representative of a class of more severe transients, whereas in the field, the training data contains transients and pressure fluctuations of all natures, resulting in a more normally distributed transient training set.

While the probability distributions obtained from the initial field training data are still valid for the second-tier SPC analysis, the conservativeness can be first increased by removing transients below a certain threshold from the training data prior to distribution fitting. Based on the results from the laboratory sensitivity analysis, a threshold of 3 was applied to the training data as a means to remove the less severe transients, while still allowing for enough variance in the distribution. Figure 4.26 shows the evolution of the distribution and probability paper plots for the Maximum, using data collected from 10 Murphy.

The thresholded data reduced the span of the original distribution, and resulted in a left-skewed distribution that did not completely follow a normal distribution, which is similar to the behaviour previously seen in the laboratory. Applying the Box-Cox transform then subsequently returned the distribution to normal. An analysis of each feature for each location was performed, and the most optimal feature sets are summarized in Table 4.2.

Comparing the feature set derived from the different field locations and from the laboratory set in Figure 4.1, it is clear that the features perform differently in different circumstances, and that training data unique to each location should be used when developing the training set to be used for the second-tier SPC analysis. Some notable changes are illustrated in Figures 4.27 and 4.28.

The laboratory data had found that RMS was amongst the more ideal features to be used for analysis. However, Figure 4.27 shows that even after using a Box-Cox transform,

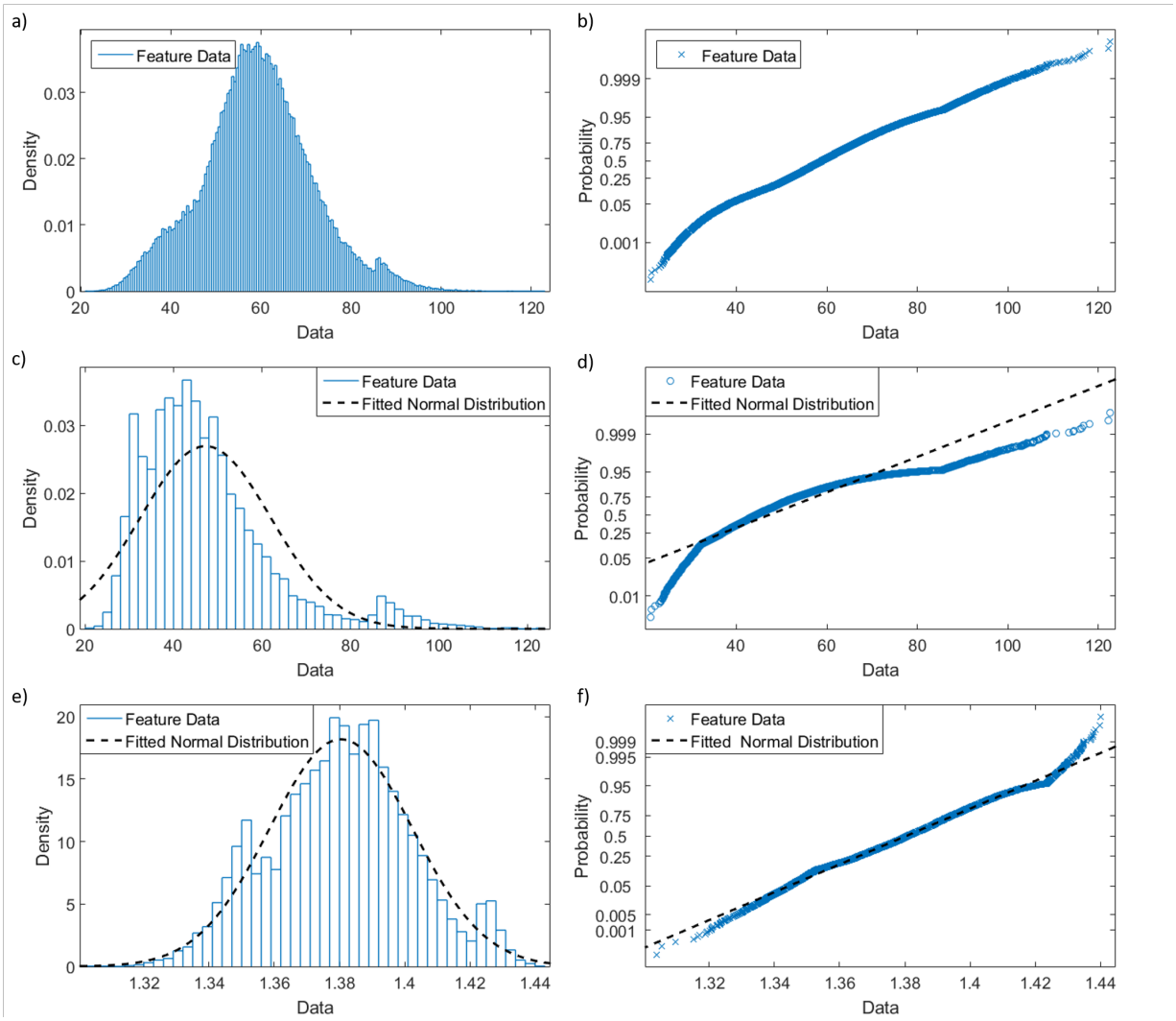

Figure 4.26: Probability distributions (left) and probability paper plots (right) of field transient Maximum data. Full training set: a) & b); threshold set to 3: c) & d); thresholds set to 3 with Box-Cox transform: e) & f).

the data set from 10 Murphy was not only right-skewed, but had a secondary peak. Figure 4.28 shows an example of a feature (Skewness) previously deemed unsuitable in the laboratory, but that closely followed a normal distribution in a field setting, even without using a transform.

Table 4.2: Abnormal transient detection feature set for the field locations

Feature	38 Keys	70 Clairfields	10 Murphy	30 Paulstown
Maximum		✓	✓	✓
Minimum		✓	✓	
Mean			✓	
Root-Mean-Square		✓		✓
Zero-crossings count	✓	✓	✓	✓
Skewness		✓	✓	
Kurtosis	✓	✓		✓
Energy		✓		✓
Entropy	✓	✓		✓
Cumulative Sum (Upper)		✓	✓	✓
Cumulative Sum (Lower)		✓	✓	

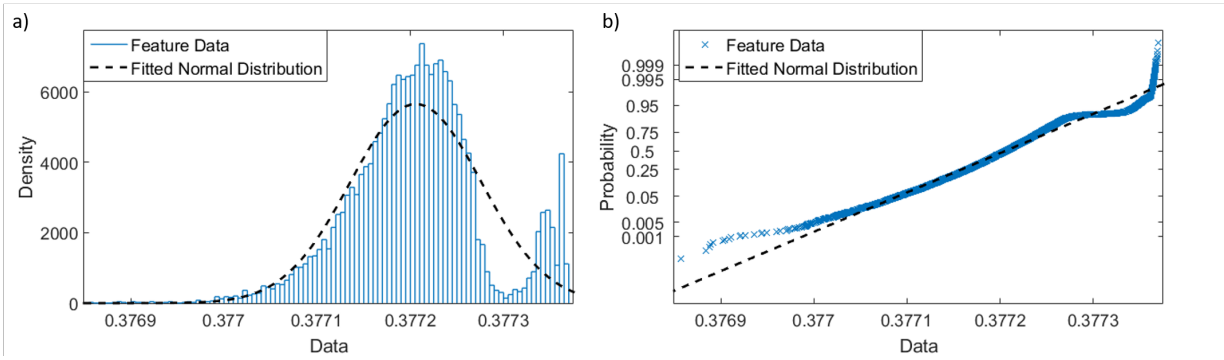

Figure 4.27: a) Probability distribution, and b) probability paper plot of Box-Cox transformed field transient RMS data from 10 Murphy.

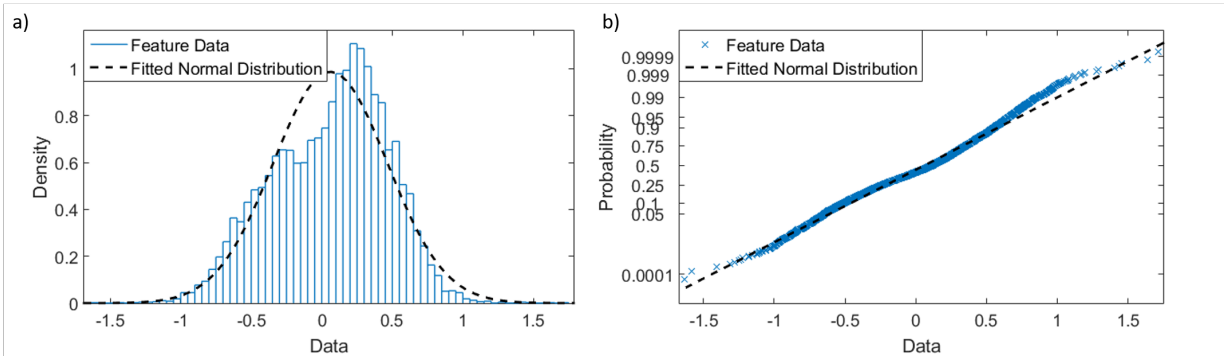

Figure 4.28: a) Probability distribution, and b) probability paper plot of field transient Skewness data from 10 Murphy.

4.3 Summary

The results of the laboratory and field tests were important for algorithm adjustment and drawing conclusions about transient behaviour in ideal and non-ideal WDNs.

Different factors contributing to algorithm performance were assessed in the laboratory, with favourable results. The pre-processing steps were shown to successfully and effectively remove unwanted signal components while retaining and emphasizing the occurrences of pressure transients. The chosen features were powerful when used in combination to identify transient activity in the system, and a voting range between 3 and 7 was determined as being optimal for the final classification step.

A higher threshold is recommended for conservative monitoring studies, where the risk for error is lower and the goal is to identify only pressure transients that may cause immediate damage to the system. Contrarily, a lower threshold would be used in order to achieve the highest possible detection rate, though it also results in a higher error rate. When monitoring for general pipe stress due to pressure, this would allow for more transient types to be encompassed in the study, including less severe or less abrupt fluctuations.

Using the system to detect known transients in a real municipal WDN, the behaviour of the pressure signals were found to be similar to the more complex laboratory cases. The algorithm was shown to be adaptable for large-scale studies under non-ideal conditions. A short-term monitoring program involving a week-long sensor deployment in various locations in a municipal DMA allowed for preliminary conclusions to be drawn about the effects of pressure changes in different areas in a WDN. As expected, very few large transients were detected in all locations, and some diurnal patterns could be seen in the frequency of

occurrence for transients in general.

A thorough validation for the abnormal transient identification process could not be feasibly conducted, but the laboratory results showed that the SPC-based method, trained with features from transients identified in the initial process, could be used to build probability distributions that lend themselves well to a sigma-based risk assessment. Further application on the field data showed that the features most suitable for the analysis varied between the different cases.

Both the laboratory and field tests showed that the algorithm can be used to illuminate the behaviours of pressure transients in municipal WDNs.

Chapter 5

Conclusions and Recommendations

5.1 Conclusions

The purpose of the research was to develop a framework that could quantify the behaviour of pressure transients in municipal WDNs and develop criteria to distinguish between normal and abnormal transients. Using different data analysis and IoT tools, the system can be used for real-time monitoring, maintenance scheduling, and long-term asset management decision making. The development of the proposed framework has achieved most of the objectives, and several conclusions can be drawn from the investigations undertaken in the laboratory and field settings.

Performance of algorithm The algorithm used for the data analysis, composed of multiple steps, was proven to successfully detect transients in both the field and laboratory settings. The data filtering was essential for rendering the data suitable for later analysis, and also for comparing data from different sets and conditions. Despite its simplicity, the SPC method was powerful for both the detection of transients, and also the potential identification of abnormal transients subsequently. The selected features were shown to note only perform well individually, but even more effectively when combined in a voting method for the final classification. It was found that the optimal feature vote threshold varied based on the purpose of a particular study, but that in the majority of cases, a threshold could be found that could maintain the error rate below 5% and the detection rate above 80%, with many cases performing even better. The methods used did not require extensive processing power and were easily implemented on the Raspberry Pi.

Additional conclusions can be drawn concerning the sensitivity of the algorithm to the effects of different conditions affecting transient propagation in a pipe. Firstly, the presence of active flow in the pipes was found to decrease the detection rate and increase the probability of error. Next, transients induced from locations farther from the sensor had a reduced chance of detection and increased the rate of false negatives in the tests. However, transients from locations too close to the sensor also increased the overall error, but instead affected the false positive rate. It was found that the proximity of a transient source to a pipe feature had a greater effect on transient propagation than the distance from a sensor. Both in the laboratory and field settings, the presence of junctions, bends, and dead-ends could either dramatically amplify or dampen the pressure wave signals. In terms of the types of transients experience in a system, pulse-type valve behaviour created stronger transients. Transients created with the abrupt opening of a valve were the most difficult to detect, followed by transients induced with the closing of a valve. It can be deduced that on a small scale, transients resulting from pressure surges are easier to detect and propagate farther and than transients resulting from pressure drops.

The methodology used for abnormal transient detection proved capable of accurately illustrating the behaviour of the transients through individual feature performance. The resulting probability distributions provide a reflection of transient properties, and are further useful when separating typical events from those worth investigating. The resulting distributions for the second-tier analysis varied by location, which indicates that case-by-case analysis should be performed in order to determine the optimal feature set.

Overall Framework Performance It was successfully proven that the use of the Raspberry Pi as the control unit for the sensor nodes is a viable solution for node-level data collection and processing. Open-source IoT solutions were integrated into the system with ease and effectively allowed data to be transmitted using the Hologram modem, and visualized using the Ubidots platform. The node-level processing allowed for smaller data transmission costs by reducing the raw data to only the most pertinent information. The system proved its capability for real-time monitoring, its usefulness for remote event detection, and value for WDN maintenance planning.

5.2 Recommendations for future work

The framework outlined in the thesis proved its effectiveness for use in transient detection. However, there are a number of areas that can be improved, as well as studies that can further add to the understanding of pressure transient behaviour and detection in WDNs.

The effect of transient source location was studied, but before large-scale node deployment, additional testing is needed in order to optimize the sensor placement. Studies should be conducted to find the average distance away from a source that an individual node can detect a transient from, to optimize sensor spacing. For both the field and laboratory, the sensors were fixed near dead-ends for practicality purposes. However, an analysis that varies sensor location, instead of transient source location, could be valuable for improving the quality of data that is used for both training and analysis.

For the algorithm, the three-sigma threshold was used across all the features during the SPC processing when identifying transients from ambient data. However, a feature-specific sensitivity analysis should be conducted in order to improve the performance of each feature and reduce the false negatives incurred by the current system.

The usefulness of the two-tier SPC process for abnormal transient identification has been shown, but more tests are needed to validate and improve the process. Also, an exploration of methods that can be used to confirm identified transients should also be undertaken. For example, the identification of a transient across multiple consecutive time intervals can be used as an indication of a correct transient identification. Additionally, the proper calibration and tracking of the true pressure in the network would allow the node to assign an accurate magnitude to each pressure change, which can factor into the estimate of the risk that the transient poses.

More field testing is needed to better adapt the system for long-term real-world usage. Ideally, tests similar to those done in the laboratory should be conducted in the field, or at the very least, tests that include inducing different transients to a field WDN should be undertaken in order to evaluate the algorithm's performance on known transients in a non-ideal setting. The addition of multiple sensors on a larger scale can also pave the way for an additional level of analysis that can correlate data from different nodes and draw conclusions based on multiple data streams.

The research summarized in the thesis can serve as an effective basis for the development of transient detection system that can be implemented widely in municipal WDNs and provide accurate, continuous, and real-time analyses of pressure behaviour.

References

Bakker, M., Jung, D., Vreeburg, J., Van De Roer, M., Lansey, K., and Rietveld, L. (2014). Detecting pipe bursts using Heuristic and CUSUM methods. *Procedia Engineering*, 70:85–92.

Bergant, A., Tijsseling, A. S., Vítkovský, J. P., Covas, D. I., Simpson, A. R., and Lambert, M. F. (2008). Parameters affecting water-hammer wave attenuation, shape and timing - Part 2: Case studies. *Journal of Hydraulic Research*, 46(3):382–391.

Boulos, P. F., Karney, B. W., Wood, D. J., and Lingireddy, S. (2005). Hydraulic transient guidelines for protecting water distribution systems. *Journal / American Water Works Association*, 97(5):111–124.

Box, G. E. P. and Cox, D. R. (2018). An Analysis of Transformations. *Journal of the Royal Statistical Society: Series B (Methodological)*.

Canada, S. (2017). Freshwater in canada: A look at canada's freshwater resources from 1971 to 2013. `https://www.statcan.gc.ca/daily-quotidien/170321/g-b001-eng.htm`. Accessed: 2018-04-09.

Dobriceanu, M., Bitoleanu, A., Popescu, M., Enache, S., and Subtirelu, E. (2008). SCADA system for monitoring water supply networks. *WSEAS Transactions on Systems*, 7(10):1070–1079.

Doty, L. A. (1996). *Statistical Process Control: Second Edition*. Industrial Press Inc., New York, New York.

Folkman, S. (2012). Water Main Break Rates In the USA and Canada. Technical report, Utah State University Buried Strucures Laboratory, Logan, Utah.

Folkman, S. (2018). Water Main Break Rates In the USA and Canada: A Comprehensive Study. *Mechanical and Aerospace Engineering Faculty Publications*, pages 1–49.

Gamboa-Medina, M. M., Ribeiro Reis, L. F., and Capobianco Guido, R. (2014). Feature extraction in pressure signals for leak detection in water networks. *Procedia Engineering*, 70:688–697.

Joukowsky, N. (1898). Über den hydraulischen Stoss in Wasserleitungsröhren. *Mémoires de l'Académie Impériale des Sciences de St.-Pétersbourg*, 9(5):Translated by O. Simin. (1904). Water Hammer. Proc.

Jung, D. and Lansey, K. (2014). Burst detection in water distribution system using the extended Kalman filter. *Procedia Engineering*, 70:902–906.

Kim, J. H., Sharma, G., Boudriga, N., and Iyengar, S. S. (2010). SPAMMS: A sensor-based pipeline autonomous monitoring and maintenance system. In *2010 2nd International Conference on COMmunication Systems and NETworks, COMSNETS 2010*.

Korteweg, D. J. (1878). Ueber die fortpflanzungsgeschwindigkeit des schalles in elastischen rhren. *Annalen der Physik*, 241(12):525–542.

Kroon, J. R., Stoner, M. A., and Hunt, W. A. (1984). Water hammer: Causes and effects. *American Water Works Association*, 76:39–45.

Mashford, J., De Silva, D., Marney, D., and Burn, S. (2009). An approach to leak detection in pipe networks using analysis of monitored pressure values by support vector machine. *NSS 2009 - Network and System Security*, pages 534–539.

Misiunas, D., Vítkovský, J., Olsson, G., Simpson, A., and Lambert, M. (2005). Pipeline Break Detection Using Pressure Transient Monitoring. *Journal of Water Resources Planning and Management*, 131(4):316–325.

Mounce, S. R. and Machell, J. (2006). Burst detection using hydraulic data from water distribution systems with artificial neural networks. *Urban Water Journal*, 3(1):21–31.

Mounce, S. R., Mounce, R. B., and Boxall, J. B. (2011). Novelty detection for time series data analysis in water distribution systems using support vector machines. *Journal of Hydroinformatics*, 13(4):672.

Mounce, S. R., Mounce, R. B., Jackson, T., Austin, J., and Boxall, J. B. (2014). Pattern matching and associative artificial neural networks for water distribution system time series data analysis. *Journal of Hydroinformatics*, 16(3):617.

Ontario MOECC (2008). Design Guidelines for Drinking-Water Systems.

Ord, S. C. (2006). Water Hammer Do We Need To Protect Against It ? How To Predict It and Prevent It Damaging Pipelines and Equipment. *Symposium Series No. 151*, 151:1–20.

Pothof, I. and Karney, B. (2013). Guidelines for Transient Analysis in Water Transmission and Distribution Systems. *Water Supply Systems Analysis - Selected Topics*, pages 1–22.

Rizzo, P. (2010). Water and wastewater pipe nondestructive evaluation and health monitoring: A review. *Advances in Civil Engineering*, 2010.

Robles, T., Alcarria, R., Martin, D., Navarro, M., Calero, R., Iglesias, S., and López, M. (2015). An IoT based reference architecture for smart water management processes. *Journal of Wireless Mobile Networks, Ubiquitous Computing, and Dependable Applications (JoWUA)*, 6(1):4–23.

Romano, M., Kapelan, Z., and Savić, D. A. (2014). Automated Detection of Pipe Bursts and Other Events in Water Distribution Systems. *Journal of Water Resources Planning and Management*, 140(4):457–467.

Sadeghioon, A. M., Metje, N., Chapman, D. N., and Anthony, C. J. (2014). SmartPipes : Smart Wireless Sensor Networks for Leak Detection in Water Pipelines. *Journal of Sensor and Actuator Networks*, 3:64–78.

Sela, L., Rasekh, A., Shafiee, M. E., and Preis, A. (2018). Characterizing pressure patterns in a water distribution network using a high-frequency monitoring system and statistical modeling. In *1st International WDSA / CCWI 2018 Joint Conference*, Kingston, ON.

Srirangarajan, S., Iqbal, M., Allen, M., Preis, A., Fu, C., Girod, L., Wong, K.-J., Lim, H. B., and Whittle, A. (2010). Real-time burst event detection in water distribution systems. In *Proceedings of the 9th ACM/IEEE International Conference on Information Processing in Sensor Networks - IPSN '10*, pages 444–445.

Starczewska, D., Collins, R., and Boxall, J. (2014). Transient behavior in complex distribution network: A case study. *Procedia Engineering*, 70:1582–1591.

Stoianov, I., Nachman, L., Whittle, A., Madden, S., and Kling, R. (2006). Sensor Networks for Monitoring Water Supply and Sewer Systems: Lessons from Boston. *Water Distribution Systems Analysis Symposium 2006*, pages 1–17.

Thorley, A. (1969). Pressure Transients in Hydraulic Pipelines. *Journal of basic engineering*, pages 453–460.

Whittle, A. J., Allen, M., Preis, A., and Iqbal, M. (2013). Sensor Networks for Monitoring and Control of Water. *The 6th International Conference on Structural Health Monitoring of Intelligent Infrastructure*, (December).

Whittle, A. J., Girod, L., Preis, A., Allen, M., Lim, H. B., Iqbal, M., Srirangarajan, S., Fu, C., and J., W. K. (2010). WATERWISE@SG: a tested for continuous monitoring of the water distribution system in Singapore. *Proc. ASCE Water Distrib. Syst. Anal.*, page 15.

APPENDICES

Appendix A

Hardware Datasheets

Honeywell

Model S

Subminiature, Flush Diaphragm Pressure Transducer

DESCRIPTION

Honeywell's full line of subminiature pressure transducers accurately measure pressure ranges from 100 psi to 15000 psi. These gage-only subminiature pressure transducers have a high natural frequency and utilize a flush diaphragm.

Temperature compensation is accomplished by using temperature-sensitive components located inside the transducers. These transducers have a small electrical zero balance circuit board which is in the lead wire (approximately 1 in x 0.087 in thick). This balance board does not have to be in the same temperature as the transducers. All transducers have four (4) active bonded strain gages arranged in a Wheatstone-bridge configuration.

FEATURES

- 100 psi to 15000 psi range
- Flush mount design
- No internal dead volume
- High frequency
- mV/V output
- 1 % accuracy
- CE approved

Model S

PERFORMANCE SPECIFICATIONS

Characteristic	Measure
Pressure ranges	
3/8-24 UNF thread	100, 150, 200, 300, 500, 750, 1000, 1500, 2000, 3000, 5000, 7500, 10000, 15000 psig
7/16-20 UNF thread	150, 300, 750, 1500, 7500, 15000 psig
Accuracy[2]	1.0 % full scale[6]
Non-linearity and hysteresis	1.0 % full scale[2]
Non-repeatability	±0.15 % full scale
Output	2 mV/V[6]
Resolution	Infinite

ENVIRONMENTAL SPECIFICATIONS

Characteristic	Measure
Temperature, operating	-54 °C to 149 °C [-65 °F to 300 °F]
Temperature, compensated	16 °C to 71 °C [60 °F to 160 °F]
Temperature effect, zero	0.01 % full scale/°F[6]
Temperature effect, span	0.02 % reading/°F[6]

ELECTRICAL SPECIFICATIONS

Characteristic	Measure
Strained gage type	Bonded foil
Excitation (calibration)	5 Vdc
Excitation (acceptable)	Up to 5 Vdc or (Vac)
Insulation resistance	5000 mOhm @ 50 Vdc
Bridge resistance	350 ohm
Shunt calibration data	Included
Electrical termination (std)	Four twisted leads (1.83 m [5 ft]) with external balance board

MECHANICAL SPECIFICATIONS

Characteristic	Measure
Media	Gases, liquids compatible with wetted parts
Overload, safe	50 % over capacity
Overload, burst	400 % full scale
Dead volume	Flush
Wetted parts material	17-4 PH stainless steel
Weight	2 oz
Case material	Stainless steel

RANGE CODES

Range Code	Available ranges
BR	100 psig
CJ	150 psig
CL	200 psig
CP	300 psig
CR	500 psig
CT	750 psig
CV	1000 psig
DJ	1500 psig
DL	2000 psig
DN	3000 psig
DR	5000 psig
DT	7500 psig
DV	10000 psig
EJ	15000 psig

OPTION CODES

Range Code	**Many range/option combinations are available in our quick-ship and fast-track manufacture programs. Please see http://sensing.honeywell.com/TMsensor-ship for updated listings.**	
Pressure ranges	100, 150, 200, 300, 500, 750, 1000, 1500, 2000, 3000, 5000, 7500, 10000, 15000 psig	
Temperature compensation	1a. 60 °F to 160 °F 1b. 30 °F to 130 °F 1c. 0 °F to 185 °F 1d. -20 °F to 130 °F	1e. -20 °F to 200 °F 1f. 70 °F to 250 °F 1g. 70 °F to 325 °F 1h. 70 °F to 400 °F 1i. -65 °F to 250 °F
Internal amplifiers	2u. Unamp., mV/V output	
Pressure ports	3/8-24 UNF 7/16-20 UNF (BP358)	
Electrical termination	Four twisted leads 1.83 m [5 ft] 6d. Microtec DR-4S-4H 4-pin (max 250 °F)[4] 6e. Integral cable: Teflon	6h. Integral cable: Silicone 6i. Integral underwater cable (max 180 °F)[4]
Special calibration	9a. 10 point (5 up/5 down) 20 % increments @ 70 °F 9b. 20 point (10 up/10 down) 10 % increments @ 70 °F	
Wetted diaphragm	10e. Iconel X-750	
Shock and vibration	44a. Shock and vibration resistance	

Subminiature, Flush Diaphragm Pressure Transducer

INSTALLATION[3]

T (thread)	A (in)[5]	B (in)	D (in) +.000/ -.002 in	O-ring	Max torque (for 17-4 PH only)
3/8-24 UNF	0.47	0.30	0.445	#11	300 in-lb
7/16-20 UNF	0.54	0.36	0.504	#12	500 in-lb

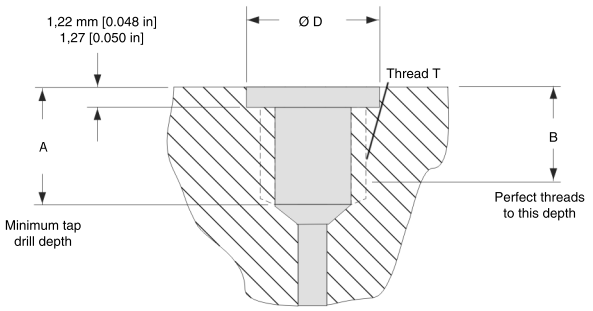

MOUNTING DIMENSIONS AND CHARACTERISTICS

Order code	T (thread)	Ø A	Ø D	B	G	Dia-phragm
BP357	3/8-24 UNF	7,87 mm [0.310 in]	12,7 mm [0.50 in]	11,43 mm [0.45 in]	17,53 mm [0.69 in]	Welded
BP358	7/16-20 UNF	9,53 mm [0.375 in]	14,22 mm [0.56 in]	12,7 mm [0.5 in]	19,05 mm [0.75 in]	Welded

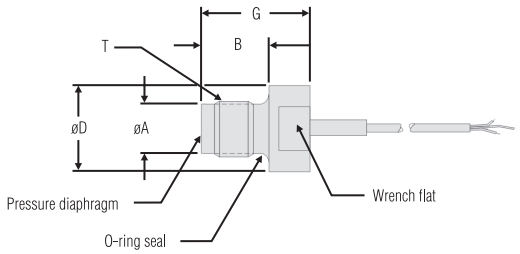

For reference only

Transducers have a small electrical balance circuit board (approximately 1.0 in long by 0.38 in wide) located in the lead wire that is two feet from the transducer body.

WIRING CODES

Wire	Cable, unamplified
Red	(+) excitation
Black	(-) excitation
Green	(-) output
White	(+) output

TYPICAL SYSTEM DIAGRAM

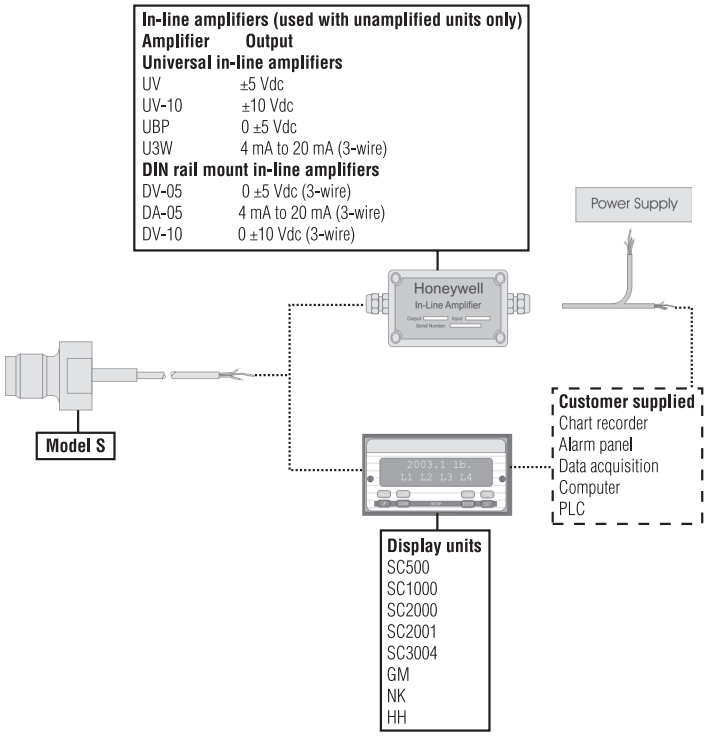

SPECIAL REQUIREMENTS (CONSULT FACTORY)

Have a special requirement? New case pressure, different cable lengths, electrical connectors, or materials? Consult our factory by calling +1 614-850-5000 (800-848-6564). Customization is key to our test and measurement business. Special outputs, wiring codes, and calibrations are all standard to us.

NOTES

1. Order code subject to change with varying thread, range and electrical termination.
2. Accuracies stated are expected for best-fit straight line for all errors, including linearity, hysteresis & non-repeatability thru zero.
3. Standard "S" type transducers have straight threads and use an O-ring for pressure sealing. To get the best seal with the O-ring on the transducer, the tapped hole should have the dimensions shown on the next page. For normal operating temperatures (-54 °C to 121 °C [-65 °F to 250 °F]) use BUNA-N (black) O-rings. For high temperatures (121 °C to 204 °C [250 °F to 400 °F) use silicone (red).
4. Only available on certain models, consult factory.
5. "A" dimension changes with different thread options. Consult factory for specifications for different thread options.
6. Consult factory for specifications for ranges less than 100 psi.

Warranty. Honeywell warrants goods of its manufacture as being free of defective materials and faulty workmanship. Honeywell's standard product warranty applies unless agreed to otherwise by Honeywell in writing; please refer to your order acknowledgement or consult your local sales office for specific warranty details. If warranted goods are returned to Honeywell during the period of coverage, Honeywell will repair or replace, at its option, without charge those items it finds defective. **The foregoing is buyer's sole remedy and is in lieu of all warranties, expressed or implied, including those of merchantability and fitness for a particular purpose. In no event shall Honeywell be liable for consequential, special, or indirect damages.**

While we provide application assistance personally, through our literature and the Honeywell web site, it is up to the customer to determine the suitability of the product in the application.

⚠ WARNING

PERSONAL INJURY

- DO NOT USE these products as safety or emergency stop devices or in any other application where failure of the product could result in personal injury.

Failure to comply with these instructions could result in death or serious injury.

⚠ WARNING

MISUSE OF DOCUMENTATION

- The information presented in this datasheet is for reference only. DO NOT USE this document as product installation information.
- Complete installation, operation and maintenance information is provided in the instructions supplied with each product.

Failure to comply with these instructions could result in death or serious injury.

Find out more

Honeywell serves its customers through a worldwide network of sales offices, representatives and distributors. For application assistance, current specifications, pricing or name of the nearest Authorized Distributor, contact your local sales office. To learn more about Honeywell's test and measurement products, call **+1-614-850-5000**, visit **www.honeywell.com/sensotec,** or e-mail inquiries to **info.tm@honeywell.com**

Sensing and Control
Honeywell
1985 Douglas Drive North
Golden Valley, MN 55422
www.honeywell.com

Honeywell

008604-2-EN IL50 GLO
August 2009

MCP3302/04

13-Bit Differential Input, Low Power A/D Converter with SPI Serial Interface

Features

- Full Differential Inputs
- 2 Differential or 4 Single-ended inputs (MCP3302)
- 4 Differential or 8 Single-ended Inputs (MCP3304)
- ±1 LSB maximum DNL
- ±1 LSB maximum INL (MCP3302/04-B)
- ±2 LSB maximum INL (MCP3302/04-C)
- Single supply operation: 4.5V to 5.5V
- 100 ksps sampling rate with 5V supply voltage
- 50 nA typical standby current, 1 µA maximum
- 450 µA maximum active current at 5V
- Industrial Temperature Range: -40°C to +85°C
- 14 and 16-pin PDIP, SOIC, and TSSOP packages
- Mixed Signal PICtail™ Demo Board (P/N: MXSIGDM) compatible

Applications

- Remote Sensors
- Battery-operated Systems
- Transducer Interface

General Description

The MCP3302/04 13-bit A/D converter features full differential inputs and low-power consumption in a small package that is ideal for battery-powered systems and remote data acquisition applications.

The MCP3302 is user-programmable to provide two differential input pairs or four single-ended inputs.

The MCP3304 is also user-programmable to configure into four differential input pairs or eight single-ended inputs.

Incorporating a successive approximation architecture with on-board sample and hold circuitry, these 13-bit A/D converters are specified to have ±1 LSB Differential Nonlinearity (DNL); ±1 LSB Integral Nonlinearity (INL) for B-grade and ±2 LSB for C-grade devices. The industry-standard SPI serial interface enables 13-bit A/D converter capability to be added to any PIC® microcontroller.

The MCP3302/04 devices feature low current design that permits operation with typical standby and active currents of only 50 nA and 300 µA, respectively. The device is capable of conversion rates of up to 100 ksps with tested specifications over a 4.5V to 5.5V supply range. The reference voltage can be varied from 400 mV to 5V, yielding input-referred resolution between 98 µV and 1.22 mV.

The MCP3302 is available in 14-pin PDIP, 150 mil SOIC and TSSOP packages. The MCP3304 is available in 16-pin PDIP and 150 mil SOIC packages. The full differential inputs of these devices enable a wide variety of signals to be used in applications such as remote data acquisition, portable instrumentation, and battery-operated applications.

Package Types

PDIP, SOIC, TSSOP

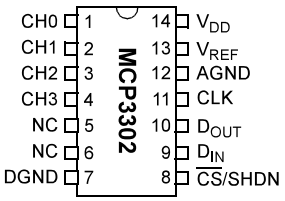

PDIP, SOIC

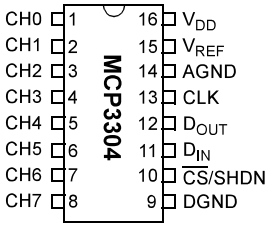

Functional Block Diagram

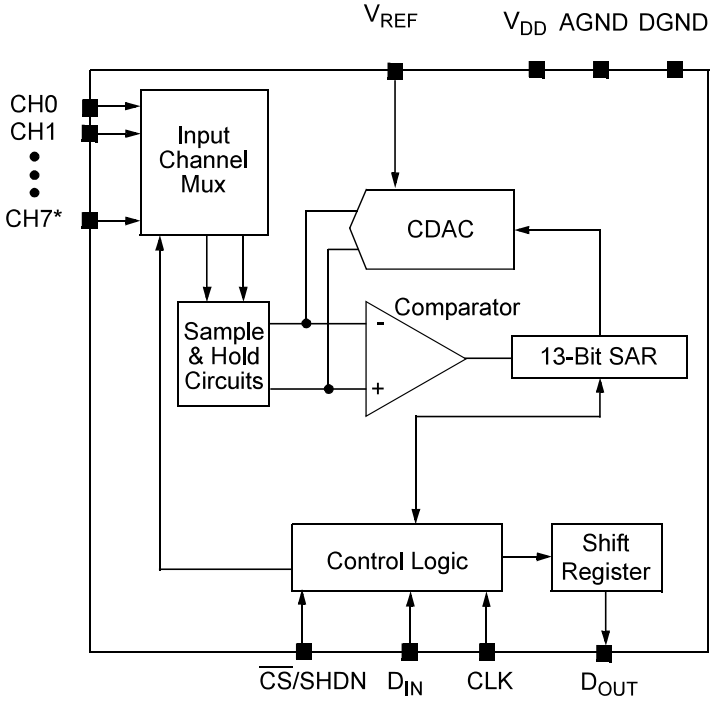

* Channels 5-7 available on **MCP3304** Only

1.0 ELECTRICAL CHARACTERISTICS

Absolute Maximum Ratings †

V_{DD}.....7.0V
All inputs and outputs w.r.t. V_{SS} ..... -0.3V to V_{DD} +0.3V
Storage temperature .....-65°C to +150°C
Ambient temp. with power applied .....-65°C to +125°C
Maximum Junction Temperature ..... 150°C
ESD protection on all pins (HBM) .....> 4 kV

† Notice: Stresses above those listed under "Maximum ratings" may cause permanent damage to the device. This is a stress rating only and functional operation of the device at those or any other conditions above those indicated in the operational listings of this specification is not implied. Exposure to maximum rating conditions for extended periods may affect device reliability.

ELECTRICAL SPECIFICATIONS

Electrical Characteristics: Unless otherwise noted, all parameters apply at V_{DD} = 5V, V_{SS} = 0V, and V_{REF} = 5V. Full differential input configuration (Figure 1-5) with fixed common mode voltage of 2.5V. All parameters apply over temperature with T_A = -40°C to +85°C (**Note 7**). Conversion speed (F_{SAMPLE}) is 100 ksps with F_{CLK} = 21*F_{SAMPLE}

Parameter	Symbol	Min	Typ	Max	Units	Conditions
Conversion Rate						
Maximum Sampling Frequency	F_{SAMPLE}	—	—	100	ksps	See F_{CLK} specification. **Note 8**
Conversion Time	T_{CONV}		13		CLK periods	
Acquisition Time	T_{ACQ}		1.5		CLK periods	
DC Accuracy						
Resolution			12 data bits + sign		bits	
Integral Nonlinearity	INL	—	±0.5	±1	LSB	MCP3302/04-B
		—	±1	±2	LSB	MCP3302/04-C
Differential Nonlinearity	DNL	—	±0.5	±1	LSB	Monotonic over temperature
Positive Gain Error		-3	-0.75	+2	LSB	
Negative Gain Error		-3	-0.5	+2	LSB	
Offset Error		-3	+3	+6	LSB	
Dynamic Performance						
Total Harmonic Distortion	THD	—	-91	—	dB	**Note 3**
Signal-to-Noise and Distortion	SINAD	—	78	—	dB	**Note 3**
Spurious Free Dynamic Range	SFDR	—	92	—	dB	**Note 3**
Common Mode Rejection	CMRR	—	79	—	dB	**Note 6**
Channel to Channel Crosstalk	CT	—	> -110	—	dB	**Note 6**
Power Supply Rejection	PSR	—	74	—	dB	**Note 4**
Reference Input						
Voltage Range		0.4	—	V_{DD}	V	**Note 2**
Current Drain		—	100	150	µA	
		—	0.001	3	µA	$\overline{CS}$ = V_{DD} = 5V

Note 1: This specification is established by characterization and not 100% tested.
2: See characterization graphs that relate converter performance to V_{REF} level.
3: V_{IN} = 0.1V to 4.9V @ 1 kHz.
4: V_{DD} =5V DC ±500 mV_{P-P} @ 1 kHz, see test circuit Figure 1-4.
5: Maximum clock frequency specification must be met.
6: V_{REF} = 400 mV, V_{IN} = 0.1V to 4.9V @ 1 kHz.
7: TSSOP devices are only specified at 25°C and +85°C.
8: For slow sample rates, see **Section 5.2 "Driving the Analog Input"** for limitations on clock frequency.
9: 4.5V - 5.5V is the supply voltage range for specified performance.

ELECTRICAL SPECIFICATIONS (CONTINUED)

Electrical Characteristics: Unless otherwise noted, all parameters apply at V_{DD} = 5V, V_{SS} = 0V, and V_{REF} = 5V. Full differential input configuration (Figure 1-5) with fixed common mode voltage of 2.5V. All parameters apply over temperature with T_A = -40°C to +85°C (**Note 7**). Conversion speed (F_{SAMPLE}) is 100 ksps with F_{CLK} = 21*F_{SAMPLE}

Parameter	Symbol	Min	Typ	Max	Units	Conditions
Analog Inputs						
Full Scale Input Span	CH0 - CH7	$-V_{REF}$	—	V_{REF}	V	
Absolute Input Voltage	CH0 - CH7	-0.3	—	V_{DD} + 0.3	V	
Leakage Current		—	0.001	±1	µA	
Switch Resistance	R_S	—	1	—	kΩ	See Figure 5-3
Sample Capacitor	C_{SAMPLE}	—	25	—	pF	See Figure 5-3
Digital Input/Output						
Data Coding Format		Binary Two's Complement				
High Level Input Voltage	V_{IH}	0.7 V_{DD}	—	—	V	
Low Level Input Voltage	V_{IL}	—	—	0.3 V_{DD}	V	
High Level Output Voltage	V_{OH}	4.1	—	—	V	I_{OH} = -1 mA, V_{DD} = 4.5V
Low Level Output Voltage	V_{OL}	—	—	0.4	V	I_{OL} = 1 mA, V_{DD} = 4.5V
Input Leakage Current	I_{LI}	-10	—	10	µA	V_{IN} = V_{SS} or V_{DD}
Output Leakage Current	I_{LO}	-10	—	10	µA	V_{OUT} = V_{SS} or V_{DD}
Pin Capacitance	C_{IN}, C_{OUT}	—	—	10	pF	T_A = +25°C, F = 1 MHz, **Note 1**
Timing Specifications:						
Clock Frequency **(Note 8)**	F_{CLK}	0.105	—	2.1	MHz	V_{DD} = 5V, F_{SAMPLE} = 100 ksps
Clock High Time	T_{HI}	210	—	—	ns	**Note 5**
Clock Low Time	T_{LO}	210	—	—	ns	**Note 5**
$\overline{CS}$ Fall To First Rising CLK Edge	T_{SUCS}	100	—	—	ns	
Data In Setup time	T_{SU}	50	—	—	ns	
Data In Hold Time	T_{HD}	50	—	—	ns	
CLK Fall To Output Data Valid	T_{DO}	—	—	125	ns	V_{DD} = 5V, see Figure 1-2
		—	—	200	ns	V_{DD} = 2.7V, see Figure 1-2
CLK Fall To Output Enable	T_{EN}	—	—	125	ns	V_{DD} = 5V, see Figure 1-2
		—	—	200	ns	V_{DD} = 2.7V, see Figure 1-2
$\overline{CS}$ Rise To Output Disable	T_{DIS}	—	—	100	ns	See test circuits, Figure 1-2 **Note 1**
$\overline{CS}$ Disable Time	T_{CSH}	475	—	—	ns	
D_{OUT} Rise Time	T_R	—	—	100	ns	See test circuits, Figure 1-2 **Note 1**
D_{OUT} Fall Time	T_F	—	—	100	ns	See test circuits, Figure 1-2 **Note 1**

Note 1: This specification is established by characterization and not 100% tested.
2: See characterization graphs that relate converter performance to V_{REF} level.
3: V_{IN} = 0.1V to 4.9V @ 1 kHz.
4: V_{DD} =5V DC ±500 mV_{P-P} @ 1 kHz, see test circuit Figure 1-4.
5: Maximum clock frequency specification must be met.
6: V_{REF} = 400 mV, V_{IN} = 0.1V to 4.9V @ 1 kHz.
7: TSSOP devices are only specified at 25°C and +85°C.
8: For slow sample rates, see **Section 5.2 "Driving the Analog Input"** for limitations on clock frequency.
9: 4.5V - 5.5V is the supply voltage range for specified performance.

ELECTRICAL SPECIFICATIONS (CONTINUED)

Electrical Characteristics: Unless otherwise noted, all parameters apply at V_{DD} = 5V, V_{SS} = 0V, and V_{REF} = 5V. Full differential input configuration (Figure 1-5) with fixed common mode voltage of 2.5V. All parameters apply over temperature with T_A = -40°C to +85°C (**Note 7**). Conversion speed (F_{SAMPLE}) is 100 ksps with F_{CLK} = 21*F_{SAMPLE}

Parameter	Symbol	Min	Typ	Max	Units	Conditions
Power Requirements:						
Operating Voltage	V_{DD}	4.5	—	5.5	V	**Note 9**
Operating Current	I_{DD}	—	300	450	µA	V_{DD}, V_{REF} = 5V, D_{OUT} unloaded
		—	200	—	µA	V_{DD}, V_{REF} = 2.7V, D_{OUT} unloaded
Standby Current	I_{DDS}	—	0.05	1	µA	$\overline{CS}$ = V_{DD} = 5.0V

Note 1: This specification is established by characterization and not 100% tested.
2: See characterization graphs that relate converter performance to V_{REF} level.
3: V_{IN} = 0.1V to 4.9V @ 1 kHz.
4: V_{DD} =5V DC ±500 mV_{P-P} @ 1 kHz, see test circuit Figure 1-4.
5: Maximum clock frequency specification must be met.
6: V_{REF} = 400 mV, V_{IN} = 0.1V to 4.9V @ 1 kHz.
7: TSSOP devices are only specified at 25°C and +85°C.
8: For slow sample rates, see **Section 5.2 "Driving the Analog Input"** for limitations on clock frequency.
9: 4.5V - 5.5V is the supply voltage range for specified performance.

TEMPERATURE CHARACTERISTICS

Electrical Specifications: Unless otherwise indicated, V_{DD} = +2.7V to +5.5V, V_{SS} = GND.

Parameters	Sym	Min	Typ	Max	Units	Conditions
Temperature Ranges						
Specified Temperature Range	T_A	-40	—	+125	°C	
Operating Temperature Range	T_A	-40	—	+125	°C	
Storage Temperature Range	T_A	-65	—	+150	°C	
Thermal Package Resistances						
Thermal Resistance, 14L-PDIP	θ_{JA}	—	70	—	°C/W	
Thermal Resistance, 14L-SOIC	θ_{JA}	—	95.3	—	°C/W	
Thermal Resistance, 14L-TSSOP	θ_{JA}	—	100	—	°C/W	
Thermal Resistance, 16L-PDIP	θ_{JA}	—	70	—	°C/W	
Thermal Resistance, 16L-SOIC	θ_{JA}	—	86.1	—	°C/W	

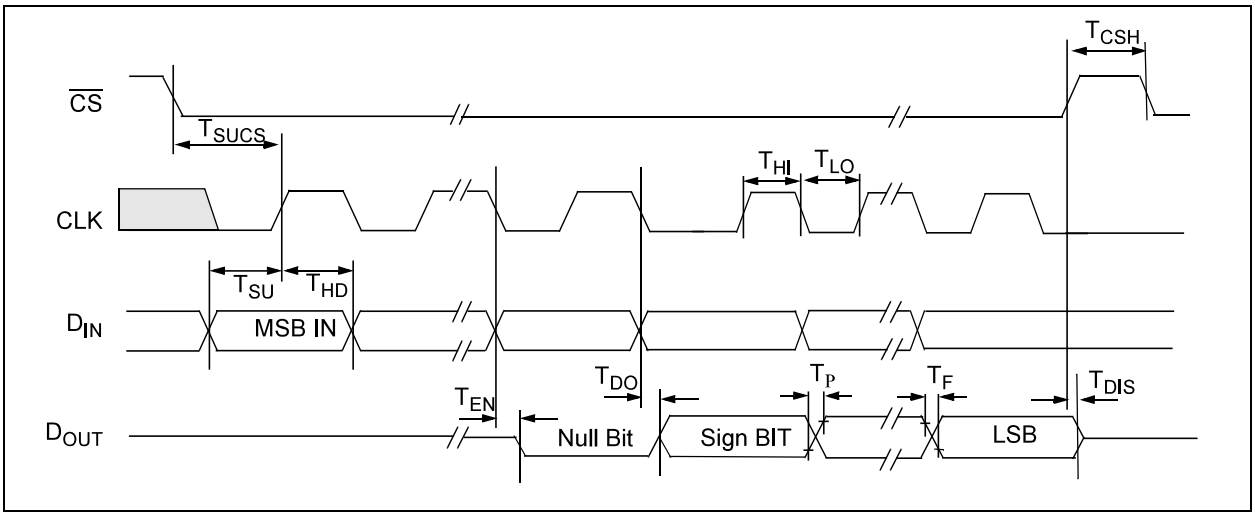

FIGURE 1-1: *Timing Parameters.*

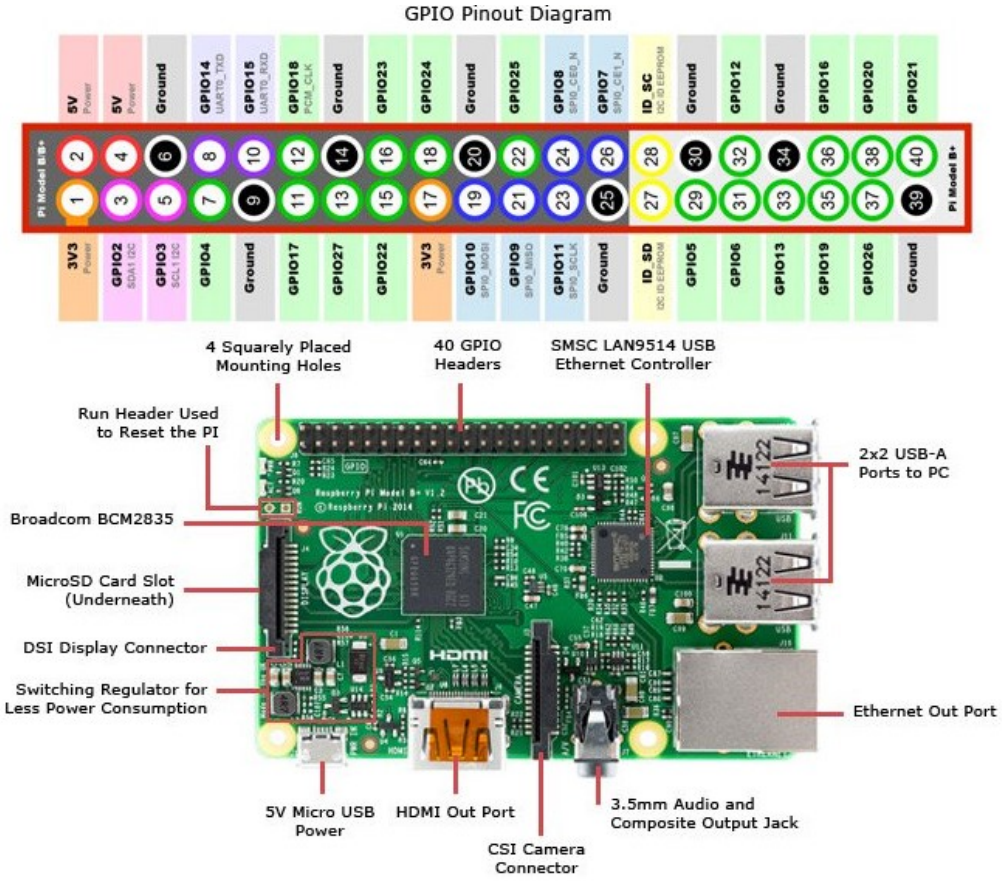

Raspberry Pi Pinouts

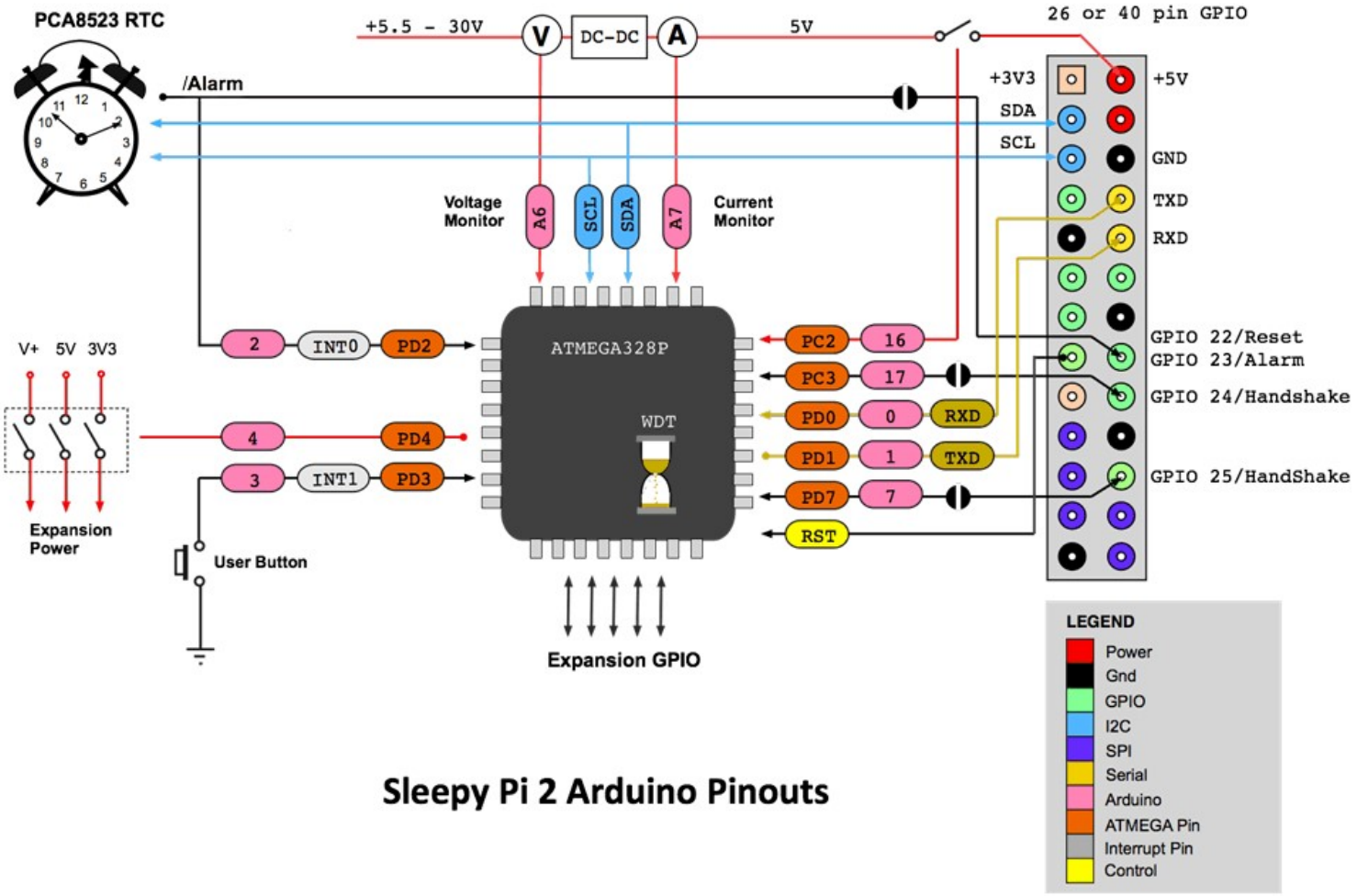

Sleepy Pi 2 Arduino Pinouts

Data Sheet and Hardware Reference

Hologram Nova Global IoT Cellular USB Modem V1.4

Issue: 04
Date: 2018-09-07

Hologram

Nova Data Sheet and Hardware Reference

TABLE OF CONTENTS

System Block Diagrams

Block diagram of the Nova board:

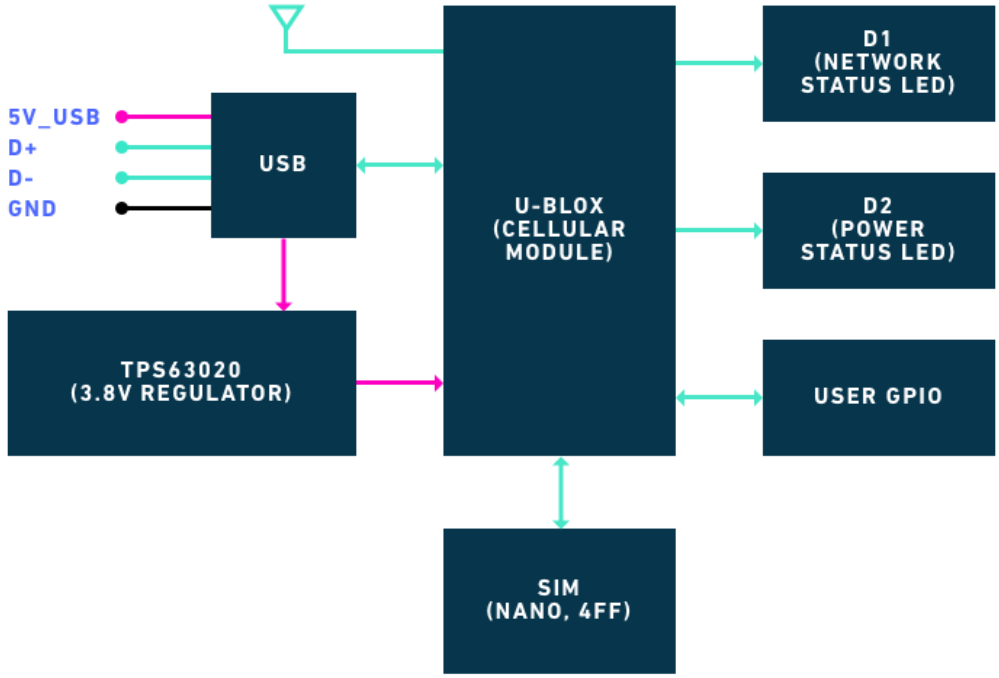

Input/Output Characteristics

USB

The Hologram Nova is designed to provide easy access to the u-blox SARA-U201 and SARA-R410-02B USB interface.

SARA series modules include a high-speed USB 2.0 compliant interface with maximum 480 Mb/s data rate. The module itself acts as a USB device and can be connected to any USB host. The USB is the suitable interface for transferring high speed data between SARA-U2 series and a host processor, available for AT commands.

The USB_D+ / USB_D- lines carry the USB serial data and signaling. The USB interface is automatically enabled by an external valid USB VBUS supply voltage (5.0 V typical) applied on the VUSB_DET pin.

For additional details, please see the following datasheets:
u-blox SARA-U201 datasheet
u-blox SARA-R4 Series datasheet

UART

At Hologram, we believe in providing an open platform for developers to build hardware. To support this mission, the Nova exposes the u-blox modem's UART interface as solderable pads on the top half of the board. For more advanced hardware devlopment, this provides direct access to the u-blox modem which runs at 1.8V

Note: USE UART PADS AT YOUR OWN RISK. Pads are directly connected to the u-blox modem so using these I/O or improperly handling the board runs the risk of damaging the u-blox modem. Additionally, we do not officially provide support this interface.

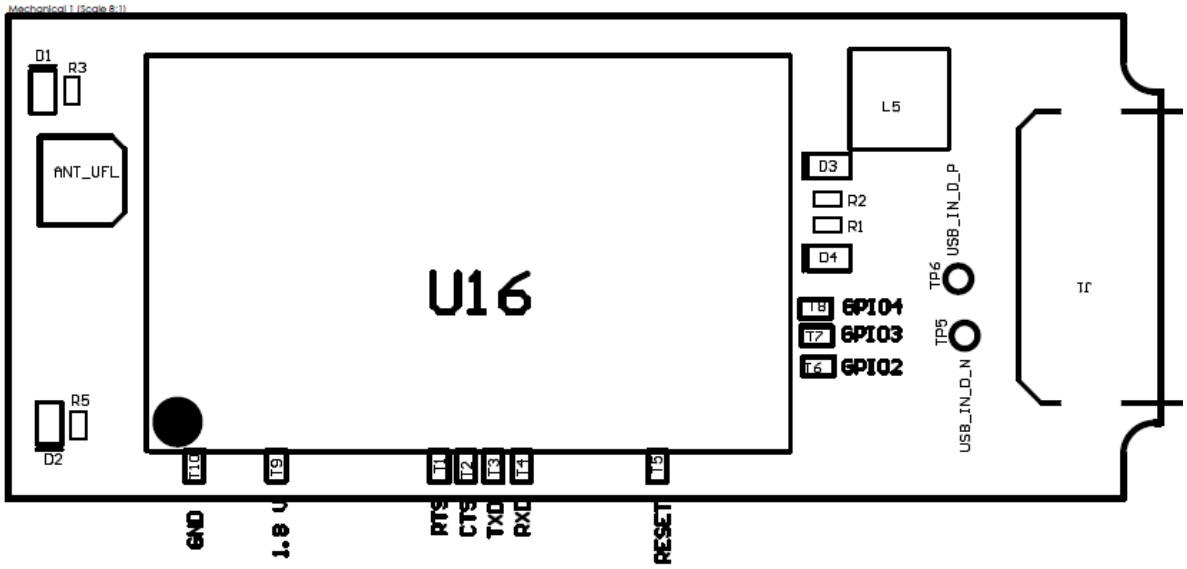

Technical Specifications

Absolute Maximum Ratings (Power Inputs)

Stressing the device above one or more of the ratings listed in the Absolute Maximum Rating section may cause permanent damage. These are stress ratings only. Operating the device at these or at any conditions other than those specified in the Operating Conditions should be avoided. Exposure to Absolute Maximum Rating conditions for extended periods may affect device reliability.

Symbol	Description	Min.	Max.	Unit
VCC, USB 5V	Input DC voltage at VCC pins	-0.30	5.50	V
USB D+/D- line	Input DC voltage at USB_D+/D- pins	-1.00	5.35	V
UBLOX_RTS UBLOX_CTS UBLOX_TXD UBLOX_RXD	Input DC voltage at u-blox digital interface pins	-0.30	3.60	V
UBLOX_RESET_N	Input DC voltage at u-blox RESET_N pin	-0.15	2.10	V
GPIO2 GPIO3 GPIO4	Input DC voltage at u-blox GPIO pins	-0.30	3.60	V

For power draw characteristics under certain cellular conditions, please view respective u-blox datasheets.

Operating Conditions

The Hologram Nova is designed to operate within temperatures between -45°C to 85°C. It is not designed to withstand material contact with moisture or any other conductors, aside from intended use of the USB. The Hologram Nova may be installed into appropriate enclosures that can protect the device from heat, cold, moisture, and humidity for Industrial use.

If handling the Nova circuit board directly, please do so in an ESD-safe environment and wear ESD protection.

Radio Specifications

The Hologram Nova platform features cellular modems which support a global list of 2G, 3G, and LTE Cat-M1/NB-IoT frequencies.

Nova 3G/2G (SARA-U201)

- 3G Bands:
  - Americas: Band 5 (850MHz), Band 2 (1900MHz)
  - Europe/Asia/Africa: Band 8 (900MHz), Band 1 (2100MHz)
- 2G Bands
  - GSM - 850MHz
  - E-GSM - 900MHz
  - DCS - 1800 MHz
  - PCS - 1900 MHz

Nova LTE-M & NB-IoT (SARA-R410M-02B)

- LTE Cat-M1/N1 Bands:
  - LTE FDD: 1, 2, 3, 4, 5, 8, 12, 13, 17, 18, 19, 20, 25, 26, 28

Mechanical Dimensions

The Hologram Nova board without an enclosure is:

- Length: 61.58 millimeters
- Width: 19.4 millimeters
- Height: 5.84 millimeters (maximum height)

Below are views of the Hologram from the top and side.

Top View:

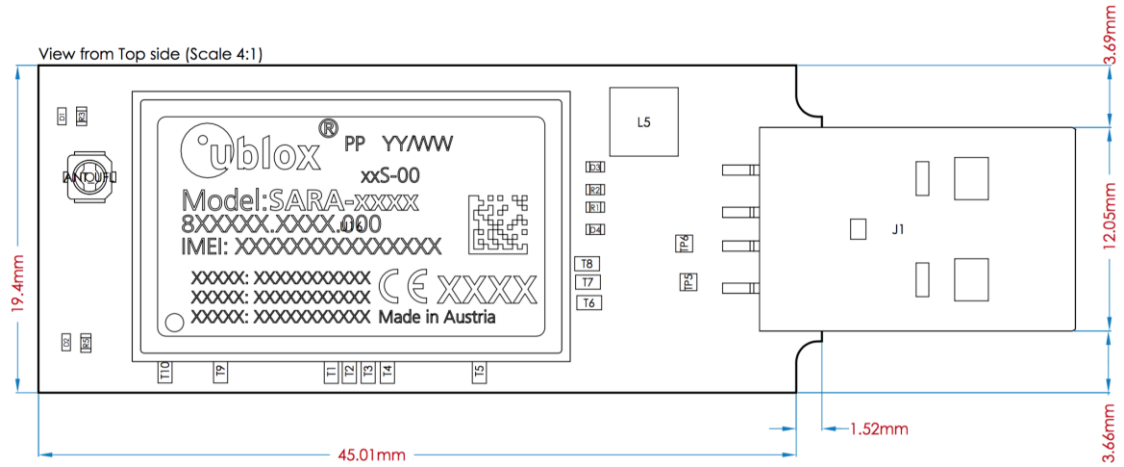

Side View:

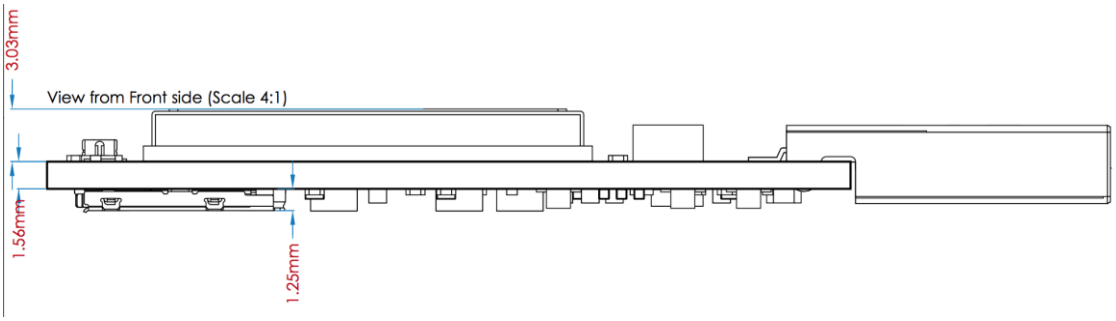

LEDs

The Nova has two clear LEDs for providing power and connectivity feedback. A power LED that represents whether the modem is on or off, and a network LED that indicates the current network status.

Note: Nova LTE-M & NB-IoT modem and Nova 3G/2G modem have same placement of LED color indicators but opposite use for power/network indication. Please use below table for reference.

MODEL	POWER LED	NETWORK LED
Nova 3G/2G	Red	Blue
Nova LTE-M & NB-IoT	Blue	Red

- Power LED status indicator (Red – 3G/2G, Blue – LTE-M & NB-IoT)
  - On: USB 5V is connected and the Nova is powered on
  - Off: USB 5V is not connected and the Nova is not powered on (modem may take up to 30s to boot up and power the LED)
- Network LED status indicator (Blue – 3G/2G, Red – LTE-M & NB-IoT)
  - On, solid: Nova connected in active data session
  - On, rapid blink: 3G network detected (3G/2G Nova Only)
  - On, double blink: 2G network detected (3G/2G Nova Only)
  - Off: No network detected
    - Make sure antenna is securely connected, positioned to receive cell signal and SIM properly inserted
    - Device can take up to 200s to detect available networks

Antennas

The Nova is made for ultimate flexibility and this extends to available antennas. Each model's included antenna characteristics are listed below:

Nova 3G/2G (SARA-U201)

- Black, flexible antenna (Sinbon A9702472)
  - Size: 37x7x1mm
  - Weight: <1g
  - Connector: U.FL
  - Mounting: Adhesive 3M tape
  - Temperature: -40C - +85C

Nova LTE-M & NB-IoT (SARA-R410)

- Black, flexible antenna (Pulse PN W3907B0100)
  - Size: 111.70x20.4x1mm
  - Weight: <1g
  - Connector: U.FL
  - Mounting: Adhesive 3M tape
  - Temperature: -40C - +85C

The Nova can also be used with additional antennas. If you'd like to use the Nova with an antenna which has an SMA connector, you need to purchase a UFL - SMA adapter.

Bill of Materials

DESIGNATOR	QUANTITY	MFG	MPN
ANT_UFL	1	Amphenol	A-1JB
C2, C6, C48	3	MURATA	GRM155R61C104KA88D
C11	1	SAMSUNG	CL10A225MQ8NNNC
C39	1	MURATA	GRM155R71C103KA01D
C34	1	Murata	GRM188R60J106ME84D
C46	1	AVX/ELCO	04025A150JAT2A
C36, C37, C38	3	MURATA	GRM188R60J226MEA0D
C41, C42, C43, C44, C45 (U201 Nova Only)	5	AVX	04025A470JAT2A
C40	1	KEMET	C0402C560J5GACTU
C47, C49, C50	3	AVX	F950J337MBAAQ2
L7	1	Murata	BLM18KG121TN1D
L5	1	Coilcraft	XFL4020-102MEC
D1	1	VISHAY	VLMB1500-GS08
D2	1	VISHAY	VLMS1500-GS08
D3, D4, D5	3	Littlefuse	PESD0402-140

DESIGNATOR	QUANTITY	MFG	MPN
L1	1	YAEGO	RC0603JR-070RL
R13	1	YAEGO	RC0402FR-071ML
R3, R5	2	YAEGO	RC0402FR-073KL
R4, R6, R7, R8	4	YAEGO	RC0402JR-0710KL
R1, R2	2	YAEGO	RC0402FR-0722RL
R11, R51	2	PANASONIC	ERJ-2GEJ104X
R12	1	YAEGO	RC0402FR-07150KL
R9	1	PANASONIC	ERJ-2GEJ471X
U16	1	U-BLOX	SARA-U260-00S
SIM1	1	GLOBAL CONNECTOR TECHNOLOGY	SIM8050-6-0-14-01-A
U2	1	TI	TPS63020DSJ
Q1, Q2, Q3, Q4	4	ON Semiconductor	MMBT3904LT1G
J1	1	MOLEX	480372200

Regulatory information

Carrier Specific Certifications

NOVA-U201 (3G/2G): AT&T, T-Mobile, PTCRB, GCF
NOVA-R410 (LTE-M & NB-IoT): Verizon ODI, AT&T, T-Mobile (In progress), PTCRB, GCF

Verizon Open Development Device #7721
AT&T Network Compatibility Record: 10bkv4QCDm

Export Control Classification Number (ECCN)

ECCNs are five character alpha-numeric designations used on the Commerce Control List (CCL) to identify dual-use items for export control purposes. An ECCN categorizes items based on the nature of the product, i.e. type of commodity, software, or technology and its respective technical parameters.

ECCN for All Nova Modems: 5A992.c

RoHS Compliance

The Nova modem family complies with the RoHS (Restriction of Hazardous Substances) directive of the European Union, EU Directive 2011/65/EU.

Harmonized Tariff Schedule Code (HTS)

HTS Code for All Nova Modems: 8517.62.0010

Interference Statement

This device complies with Part 15 of the FCC Rules and Industry Canada licence-exempt RSS standards. Operation is subject to the following two conditions: (1) This device may not cause harmful interferences, and (2) this device must accept any interference received, including interference that may cause undesired operation.

FCC & IC Compliance

If the modem's antenna is located farther than 20cm from the human body and there are no proximate transmitters, the FCC/IC approvals of the constituent u-blox SARA-U201 or SARA-R410-02B can be reused by the end product.

Should the modems antenna be mounted closer than 20cm from the human body or if there are proximate transmitters, additional FCC/IC testing may be required for the end product.

Nova 3G/2G & Nova LTE-M & NB-IoT modems make use of the underlying u-blox module's FCC & IC identification numbers below.

MODEL	FCC ID	IC ID (CERTIFICATION NUMBER)
Nova 3G/2G	XPY1CGM5NNN	8595A-1CGM5NNN
Nova LTE-M & NB-IoT	XPY2AGQN4NNN	8595A-2AGQN4NNN

Additionally, all Nova modems are compliant with FCC Part 15 Class B

Modification Statement

Hologram has not approved any changes or modifications to this device by the user. Any changes or modifications could void the user's authorization to operate the equipment.

End Product Labeling Requirements

End products utilizing Nova 3G/2G modems should be labeled with the following information:

> Device Uses Approved Radio: NOVA-U201
>
> Contains FCC ID: XPY2AGQN4NNN
> Contains IC: 8595A-1CGM5NNN
>
> This device complies with Part 15 of the FCC Rules and Industry Canada licence-exempt RSS standards. Operation is subject to the following two conditions: (1) This device may not cause harmful interferences, and (2) this device must accept any interference received, including interference that may cause undesired operation.

End products utilizing Nova LTE-M &NB-IoT modems should be labeled with the following information:

> Device Uses Approved Radio: NOVA-R410
>
> Contains FCC ID: XPY2AGQN4NNN
> Contains IC: 8595A-2AGQN4NNN
>
> This device complies with Part 15 of the FCC Rules and Industry Canada licence-exempt RSS standards. Operation is subject to the following two conditions: (1) This device may not cause harmful interferences, and (2) this device must accept any interference received, including interference that may cause undesired operation.

Appendix B

List of Features

Feature	Calculation	Use
Maximum	$x_{mx} = max(x_i)$	Largest positive peak
Minimum	$x_{mn} = min(x_i)$	Largest negative peak
Mean	$x_{me} = \frac{\sum_{i=1}^{n} x_i}{n}$	Average
Skewness	$x_{sk} = \frac{\sum_{i=1}^{n}(x_i - x_{me})^3}{(n-1)x_{rm}^3}$	Indicator of asymmetry
Kurtosis	$x_{kt} = \frac{\sum_{i=1}^{n}(x_i - x_{me})^4}{(n-1)x_{rm}^4}$	Indicator of 'tailed-ness' of distribution
Root-mean-square	$x_{rm} = \left(\frac{1}{n}\sum_{i=1}^{n} x_i^2\right)^{1/2}$	Measure of magnitude
Energy	$x_{en} = \sum_{i=1}^{n} x_i^2$	Secondary measure of magnitude
Upper CUSUM	$x_{cu} = \sum_{i=1}^{n} max[0, x_i - (u_i + K_u)]$	Useful for change detection
Lower CUSUM	$x_{cl} = \sum_{i=1}^{n} max[0, (u_i - K_u) - x_i]$	Useful for change detection
Zero-crossings count	$x_{zc} = \sum_{i=2}^{n} I(x_i * x_{i-1} < 0)$	Detects changes in signal phase
Entropy	$x_{et} = -\sum_{i=1}^{n} P_i \log_2 P_i; P_i = \frac{x_i^2}{\sum_{i=1}^{n} x_i^2}$	Unpredictability